



Variable Stars Observed in the Galactic Disk by AST3-1 from Dome A, Antarctica

Lingzhi Wang^{1,2,3}, Bin Ma^{1,3}, Gang Li⁴, Yi Hu^{1,3}, Jianning Fu⁴, Lifan Wang^{3,5,6}, Michael C. B. Ashley⁷, Xiangqun Cui^{3,8}, Fujia Du^{3,8}, Xuefei Gong^{3,8}, Xiaoyan Li^{3,8}, Zhengyang Li^{3,8}, Qiang Liu^{1,3}, Carl R. Pennypacker⁹, Zhaohui Shang^{1,3,10}, Xiangyan Yuan^{3,8}, Donald G. York¹¹, and Jilin Zhou^{3,12}

¹ Key Laboratory of Optical Astronomy, National Astronomical Observatories, Chinese Academy of Sciences, Beijing 100012, China; wanglingzhi@bao.ac.cn

² Chinese Academy of Sciences South America Center for Astronomy, Camino EL Observatorio 1515, Las Condes, Santiago, Chile

³ Chinese Center for Antarctic Astronomy, Nanjing 210008, China

⁴ Department of Astronomy, Beijing Normal University, Beijing, 100875, China

⁵ Purple Mountain Observatory, Chinese Academy of Sciences, Nanjing 210008, China

⁶ Mitchell Institute for Fundamental Physics & Astronomy, Department of Physics & Astronomy, Texas A&M University, College Station, TX 77843, USA

⁷ School of Physics, University of New South Wales, NSW 2052, Australia

⁸ Nanjing Institute of Astronomical Optics and Technology, Nanjing 210042, China

⁹ Center for Astrophysics, Lawrence Berkeley National Laboratory, Berkeley, CA, USA

¹⁰ Tianjin Normal University, Tianjin 300074, China

¹¹ Department of Astronomy and Astrophysics and Enrico Fermi Institute, University of Chicago, Chicago, IL 60637, USA

¹² School of Astronomy and Space Science and Key Laboratory of Modern Astronomy and

Astrophysics in Ministry of Education, Nanjing University, Nanjing 210093, China

Received 2016 March 20; revised 2016 December 13; accepted 2016 December 31; published 2017 February 9

Abstract

AST3-1 is the second-generation wide-field optical photometric telescope dedicated to time-domain astronomy at Dome A, Antarctica. Here, we present the results of an *i*-band images survey from AST3-1 toward one Galactic disk field. Based on time-series photometry of 92,583 stars, 560 variable stars were detected with *i* magnitude ≤ 16.5 mag during eight days of observations; 339 of these are previously unknown variables. We tentatively classify the 560 variables as 285 eclipsing binaries (EW, EB, and EA), 27 pulsating variable stars (δ Scuti, γ Doradus, δ Cephei variable, and RR Lyrae stars), and 248 other types of variables (unclassified periodic, multiperiodic, and aperiodic variable stars). Of the eclipsing binaries, 34 show O'Connell effects. One of the aperiodic variables shows a plateau light curve and another variable shows a secondary maximum after peak brightness. We also detected a complex binary system with an RS CVn-like light-curve morphology; this object is being followed-up spectroscopically using the Gemini South telescope.

Key words: binaries: eclipsing – catalogs – methods: data analysis – stars: variables: general – surveys – techniques: photometric

Supporting material: machine-readable tables, tar.gz file

1. Introduction

Time-domain astronomy is the investigation of astronomical objects as a function of time, and it has long been a source of interesting and unexpected discoveries. Ongoing and new ground- and space-based large synoptic sky surveys such as the (intermediate) Palomar Transient Factory (Law et al. 2009; Rau et al. 2009), the SkyMapper Telescope (Keller et al. 2007), and the Large Synoptic Survey Telescope (LSST Science Collaboration et al. 2009) after its first light in 2020¹³ are exploring or will explore new regions of parameter space in terms of depth and temporal coverage.

The Antarctic plateau offers a number of unique advantages for precision ground-based time-domain astronomy, such as the ability to observe continuously during winter, low scintillation noise, excellent seeing above a very low boundary layer, low airmass variations, low aerosols, low water vapor, more stable atmospheric transmission, wider wavelength windows, and a dark sky in the infrared (Lawrence et al. 2004, 2006, 2008; Kulesa et al. 2008; Moore et al. 2008; Aristidi et al. 2009; Bonner et al. 2010; Burton 2010; Sims et al. 2010; Yang et al. 2010; Zou et al. 2010; Lascaux et al. 2011; Pei et al. 2011, 2012; Tremblin et al.

2011; Giordano et al. 2012; Sims et al. 2012a, 2012b; Storey 2013; Ashley 2013; Hu et al. 2014; Yang et al. 2016). There is thus considerable interest in overcoming the technical challenges of operating in Antarctica, so that the advantages for astronomy can be realized (Kulesa et al. 2008; Tothill et al. 2008; Crouzet et al. 2010; Chapellier et al. 2016; Mékarnia et al. 2016).

Dome A (latitude 80°22'02"S, longitude 77°21'11"E, elevation 4093 m above the sea level) is the highest region on the Antarctic plateau and is being used for a series of three increasingly ambitious optical survey telescopes (Yang et al. 2009; Gong et al. 2010). The first optical telescope was called CSTAR (the Chinese Small Telescope ARray; Yuan et al. 2008) with an effective aperture of 10 cm and a field of view (FOV) of 20 deg². It was installed at Dome A in 2008 January and produced a three-year photometric data set. A number of studies of stellar variability have been published (Zhou et al. 2010a, 2010b, 2013; Huang et al. 2013, 2015; Meng et al. 2013; Wang et al. 2011, 2012, 2013a, 2013b, 2014a, 2014b, 2015; Fu et al. 2014; Qian et al. 2014; Oelkers et al. 2015, 2016; Yang et al. 2015; Zong et al. 2015; Liang et al. 2016). The second-generation optical telescope at Dome A is called AST3, which in turn consists of three telescopes, each with an entrance pupil diameter of 0.5 m and a FOV of 4.3 deg² (Cui et al. 2008; Yuan & Su 2012; Yuan et al. 2014, 2015). The first two of the AST3

¹³ <https://www.lsst.org/about/timeline>

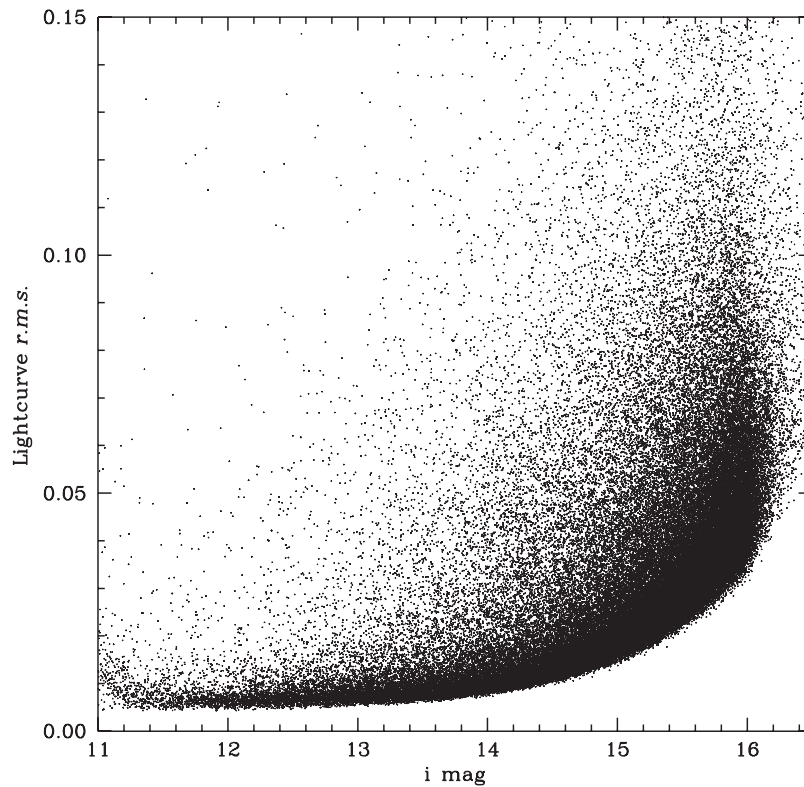


Figure 1. Rms magnitude range of light curves of 92,583 stars with at least 20% measurements.

Table 1
Log of Observations

Date	# Images	Total Exp. Time (hr)
2012		
Mar 28	156	2.56
Apr 24	6	0.02
Apr 25	515	6.91
Apr 26	516	6.03
Apr 27	58	0.83
Apr 28	368	5.64
Apr 29	666	6.55
Apr 30	750	6.25
May 01	488	4.07
Total	3523	38.86

telescopes—AST3-1 (Li et al. 2012a, 2012b; Wen et al. 2012) and AST3-2—were installed at Dome A in 2012 and 2015 January, respectively. The third AST3 telescope is planned to be installed in 2017 and will have a *K*-band infrared camera. The third-generation optical/infrared telescope destined for Dome A is called KDUST (the Kunlun Dark Universe Survey Telescope; Jia & Zhang 2012, 2013; Yuan et al. 2013; Zhu et al. 2014; Burton et al. 2016; Li et al. 2016; Xu et al. 2016), which has an aperture of 2.5 m and a FOV of ~ 2.3 deg² (Yuan et al. 2013); KDUST is expected to be operational at Dome A after 2022.

The three AST3 telescopes were originally conceived as multiband survey telescopes, with each telescope having a fixed filter to reduce the risk of mechanism failure. Their main sky survey area is a zenith distance less than 70° (Yuan & Su 2012). Meanwhile, other factors for observations are also taken into account, including the altitude and phase of the Moon, the angular distance between the telescope pointing and the Moon,

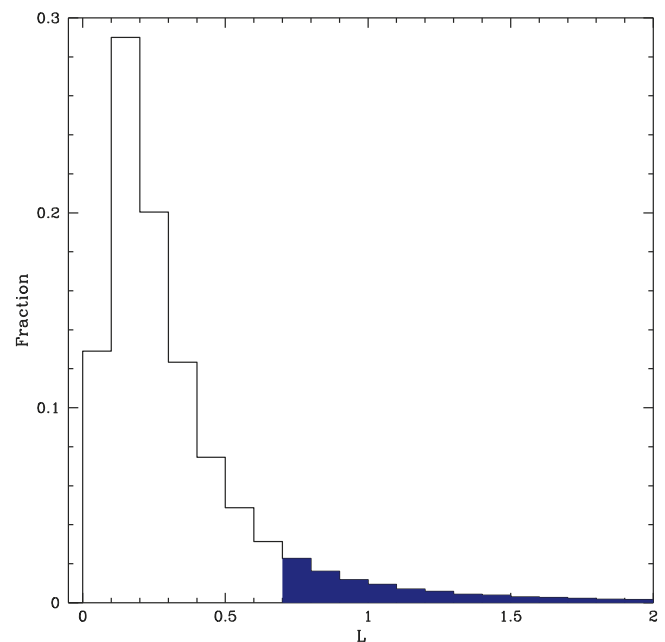


Figure 2. Distribution of the Welch–Stetson variability statistic L (Welch & Stetson 1993; Stetson 1996) for the 92,583 brightest stars in the AST3-1 sample.

and the altitude of the Sun (Shang et al. 2012). To operate the AST3 at remote Dome A, an improved version of PLATO (an automated observatory platform for CSTAR and other earlier instruments¹⁴), PLATO-A was designed to offer about 1 kW

¹⁴ <http://mcba11.phys.unsw.edu.au/~plato-a>

Table 2
Variable Stars

(1) ID	(2) R.A.	(3) Decl.	(4) i (mag ^a)	(5) L	(6) Period ^b (days)	(7) χ^2	(8) Amp (mag)	(9) T_0^c	(10) Type ^d	(11) Note ^e
AST00006	10:50:18.48	-61:50:54.4	15.31	0.88	0.15	...	VAR	...
AST00391	10:50:21.84	-62:11:29.2	14.71	6.99	3.024214983 (144)	0.48	0.59	...	DCEP	...
AST00424	10:50:20.62	-62:01:08.1	13.13	0.67	2.455793858 (602)	0.26	0.04	15429.813526	EW-OC PER	...
AST00626	10:50:23.52	-62:00:18.8	14.56	1.47	2.310849190 (88)	0.63	0.24	15430.484424	EA	...
AST00651	10:50:23.85	-62:27:13.9	14.35	0.86	0.13	...	VAR	...
AST00723	10:50:20.70	-62:17:13.6	12.90	4.76	0.23	...	VAR	...
AST00769	10:50:25.00	-62:10:13.5	15.21	1.20	0.17	...	VAR	...
AST01150	10:50:27.04	-62:47:05.8	13.84	1.33	1.342747211 (118)	0.32	0.08	15428.847705	EW-OC	...
AST01289	10:50:27.57	-61:59:12.4	13.11	0.75	1.351890564 (204)	0.31	0.05	...	PER	...
AST01361	10:50:28.59	-62:27:36.5	14.95	0.85	0.324106067 (18)	0.98	0.08	15428.167041	PER	...

Notes.^a The i -band mean magnitude (not an intensity mean).^b The median value of the period and its standard deviation in brackets in units of 10^{-9} days via MCMC simulation, when applicable.^c Epoch of minimum light since 1970-01-01 00:00:00 UTC, if possible.^d Type: VAR, objects with statistically significant variabilities, but not showing periodic behaviors; EW, W Ursae Majoris-type binary; EB, β Lyrae-type binary; EA, Algol-type binary; EW-OC, EW binary with O'Connell effect; EB-OC, EB binary with O'Connell effect; DCEP, δ Cephei variable; DS, δ Scuti variable; GD, γ Doradus variable; PER, unclassified periodic; MP, multiperiodic; RRAB, RRab Lyrae variable; RRC, RRC Lyrae variable; the “|” sign is the separator of two different alternatives.^e Note: [A], AAVSO variable; [O], OGLE-III variable; [G], GDS variable.

(This table is available in its entirety in machine-readable form.)

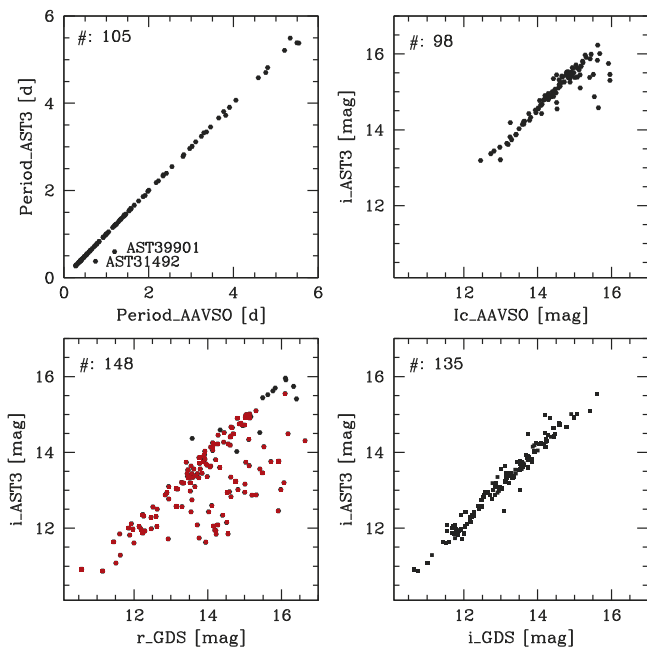


Figure 3. Top left: the measured periods for 105 variable stars from AST3-1 compared to the periods given in the AAVSO database; top right: the measured i magnitude for 98 variable stars from AST3-1 compared to the Cousins’ i_c magnitude given in the AAVSO database; bottom left: black solid circles show the i magnitude for 148 variable stars from AST3-1 compared to the Sloan r magnitude given in the GDS catalog (red squares for 135 out of 148 stars with both r - and i -band magnitudes); bottom right: i magnitude for 135 variable stars from AST3-1 compared to the Sloan i magnitude given in the GDS catalog.

power source for AST3 (Lawrence et al. 2009; Ashley et al. 2010; Shang et al. 2012).

The three main science goals for AST3 are the early detection of supernovae, exoplanet transit searches, and stellar

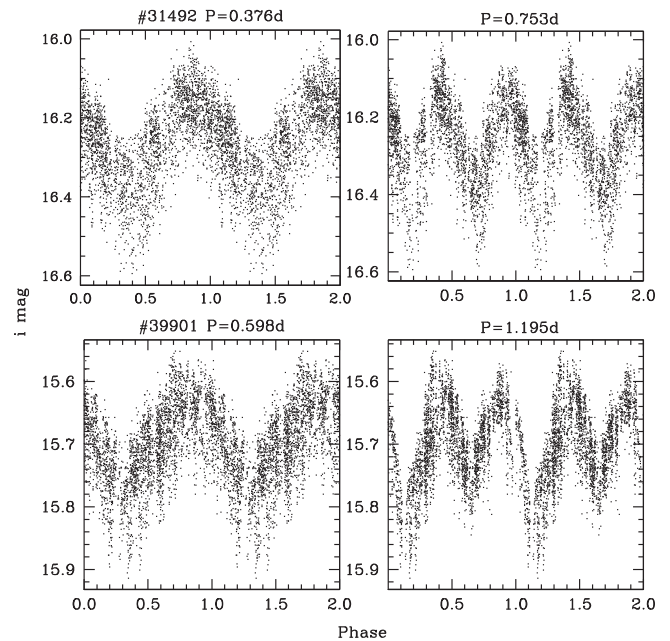


Figure 4. Phased light curves were folded by periods from AST3-1 (left panels) and from the AAVSO database (twice that from AST3-1, right panels) for AST31492 and 39901; the AST3-1 periods are more likely to be correct.

variability (Cui et al. 2008). The first AST3 telescope (AST3-1) was successfully deployed to Dome A in 2012 January, and $\sim 16,000$ scientific frames were collected from 2012 March 16 to May 7, with a total exposure time of 189 hr. After that, AST3-1 unfortunately stopped work due to a malfunctioning power distribution box. Of the $\sim 16,000$ images obtained, 4,000 were of 500 fields mainly surveyed for supernova templates;

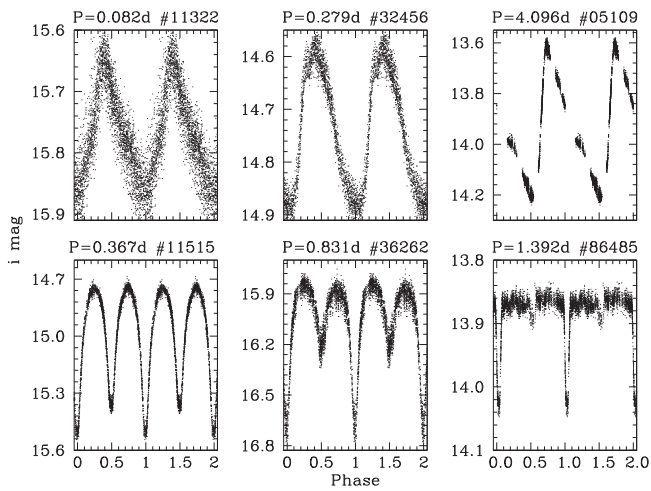


Figure 5. Phased light curves for six typical periodic variable stars. The periods and AST IDs are listed above each panel. Top row (from left to right): δ Scuti, RR1yr c-type star, and δ Cepheid; bottom row (from left to right): eclipsing binaries of W UMa-type (EW), β Lyrae-type (EB), and Algol-type (EA) configurations.

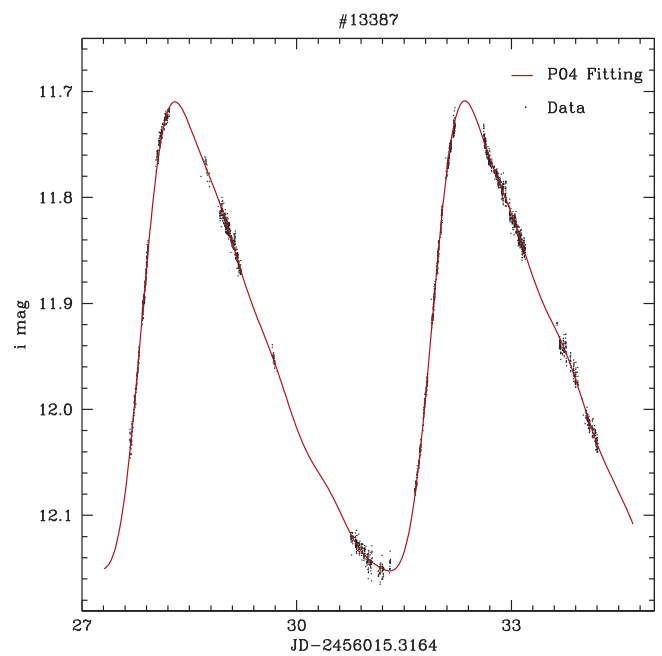


Figure 7. Observed light curves of the known δ Cepheid GS Car (AST13387) in i band (black points) and the fitting curves with the fundamental frequency and the harmonics (red curves).

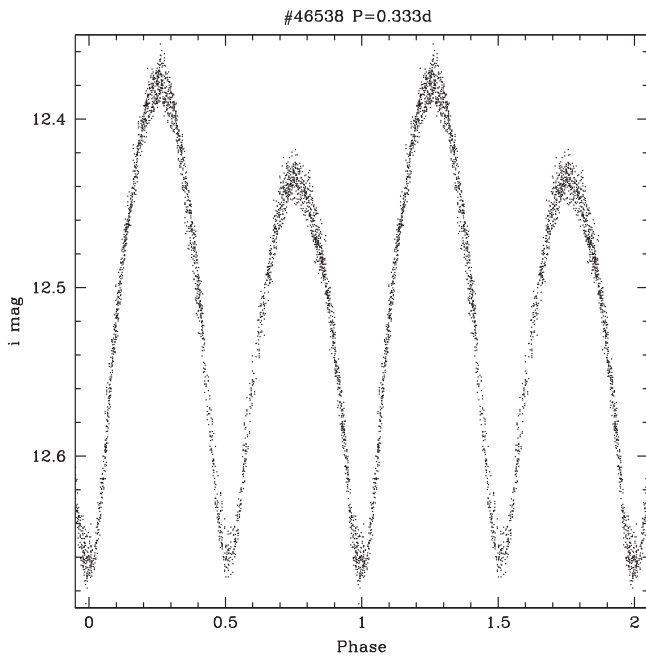


Figure 6. The phased diagram of AST46538, which has the most significant O'Connell effect in our sample. Its ID and orbital period are marked in the title.

Table 3
Distribution of Variable Star Types

Variable Type	N	%	$N(\text{new})$
Binaries (EW, EB, EA)	285	50.9	143
Pulsators (DS, GD, DCEP, R Rab, RRc)	27	4.8	16
Others (PER, MP, VAR)	248	44.3	180

~ 4700 images were of the center of the Large Magellanic Cloud, and ~ 3400 images covered eight Galactic disk fields to study Wolf-Rayet stars, and one Galactic disk field was used primarily to search for transiting exo-planets. This latter field

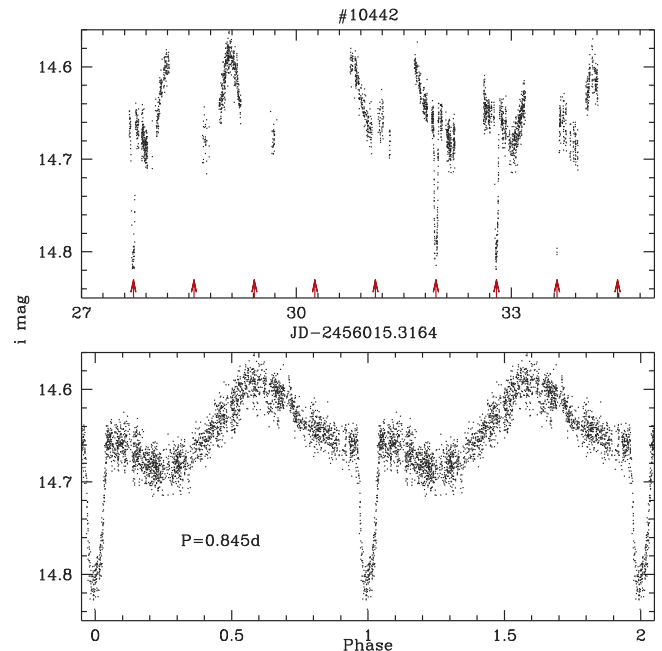


Figure 8. Top panel: light curve of AST10442 in the i band, showing an RS CVn-like pattern with a period of 0.845 days, and a clearly detected prominent primary minimum (marked with arrows in the top plot). Bottom panel: phased light curve of AST10442 folded by the period of 0.845 days.

had the highest number of observations, and so was also suited to study stellar variability, which is the subject of this paper. The field was centered at $l = 289^{\circ}6347$, $b = -1^{\circ}5718$, and was monitored in i band with 3523 images over 8 days with a total exposure time of 38.9 hr. Of these 38.9 hr, 157 frames totalling 2.6 hr were observed on March 28, and 3366 frames totalling 36.3 hr were from April 24 to May 1 (Table 1). The distribution of the 36.3 hr over the 7 days of observations can

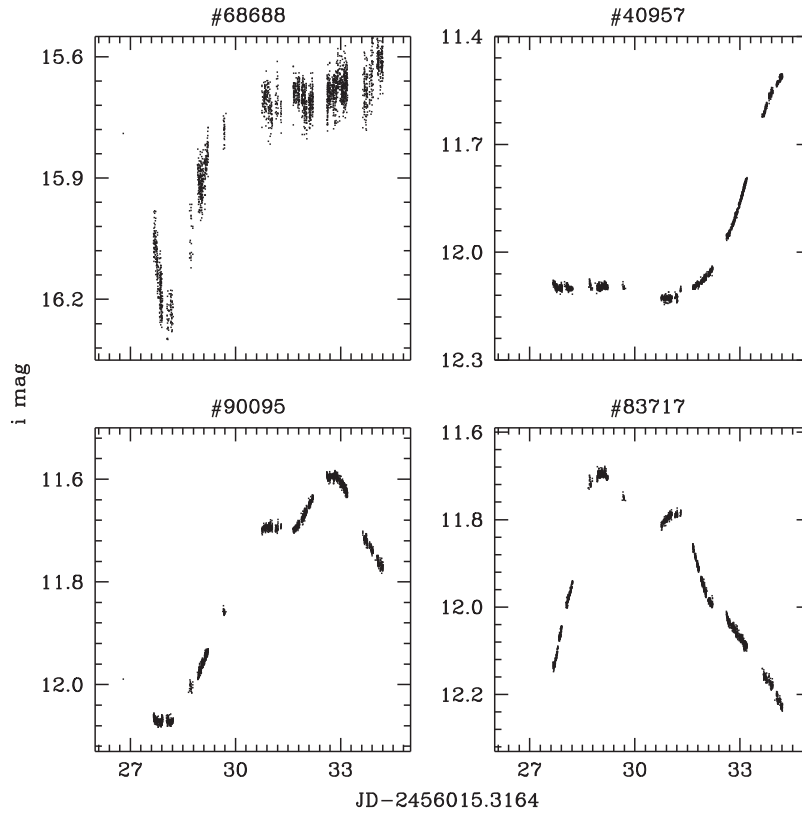


Figure 9. Light curves of four unclassified aperiodic variable stars with the largest variability amplitudes.

Table 4
Identifications for the 221 Variables in Common

(1) AST3	(2) AAVSO	(3) GDS	(4) OGLE-III or others
AST01736	...	GDS_J1050304-613526	...
AST02497	310338	...	OGLE-GD-ECL-03652
AST03182	310357	...	OGLE-GD-ECL-03671
AST04554	...	GDS_J1050526-615847	...
AST05016	...	GDS_J1050463-602841	...
AST05512	310418	...	OGLE-GD-ECL-03733
AST06264	310438	GDS_J1051045-612147	OGLE-GD-ECL-03753
AST06935	310450	...	OGLE-GD-ECL-03765
AST07839	...	GDS_J1051142-614524	...
AST08666	92320	GDS_J1051153-603208	ASAS J105115-6032.1

(This table is available in its entirety in machine-readable form.)

be seen from the time-series plots. Gaps in the observations were mainly due to the AST3-1 telescope being pointed to other fields. The observations, the data reduction, and the time-series photometry are briefly described in Section 2. The catalog of variable stars and preliminary statistics of the variable star types are presented in Section 3. Our results are summarized in Section 4.

2. Observations and Data Reduction

2.1. Observations

AST3 (Cui et al. 2008; Yuan et al. 2014, 2015) was conceived as three telescopes, each equipped with one of three SDSS g , r ,

and i filters. Each telescope has an entrance pupil aperture of 0.5 m and a wide FOV of 4.3 deg^2 , and is equipped with a $10 \text{ K} \times 10 \text{ K}$ frame transfer STA1600FT CCD (charge coupled device) camera. The CCD detector is divided into frame store regions at the top and bottom quarters and an image area in the central half in order to operate in frame transfer mode without a shutter—this is part of our risk-mitigation strategy of eliminating mechanisms as far as possible, since the telescope has to operate entirely remotely for 11 months of the year with no possibility of repairs being carried out. The image area of the CCD has 16 readouts, each with 1320×2640 pixels, including an overscan region of 180 columns on the readout electronics end. More details about the AST3 CCD performance, data system, and

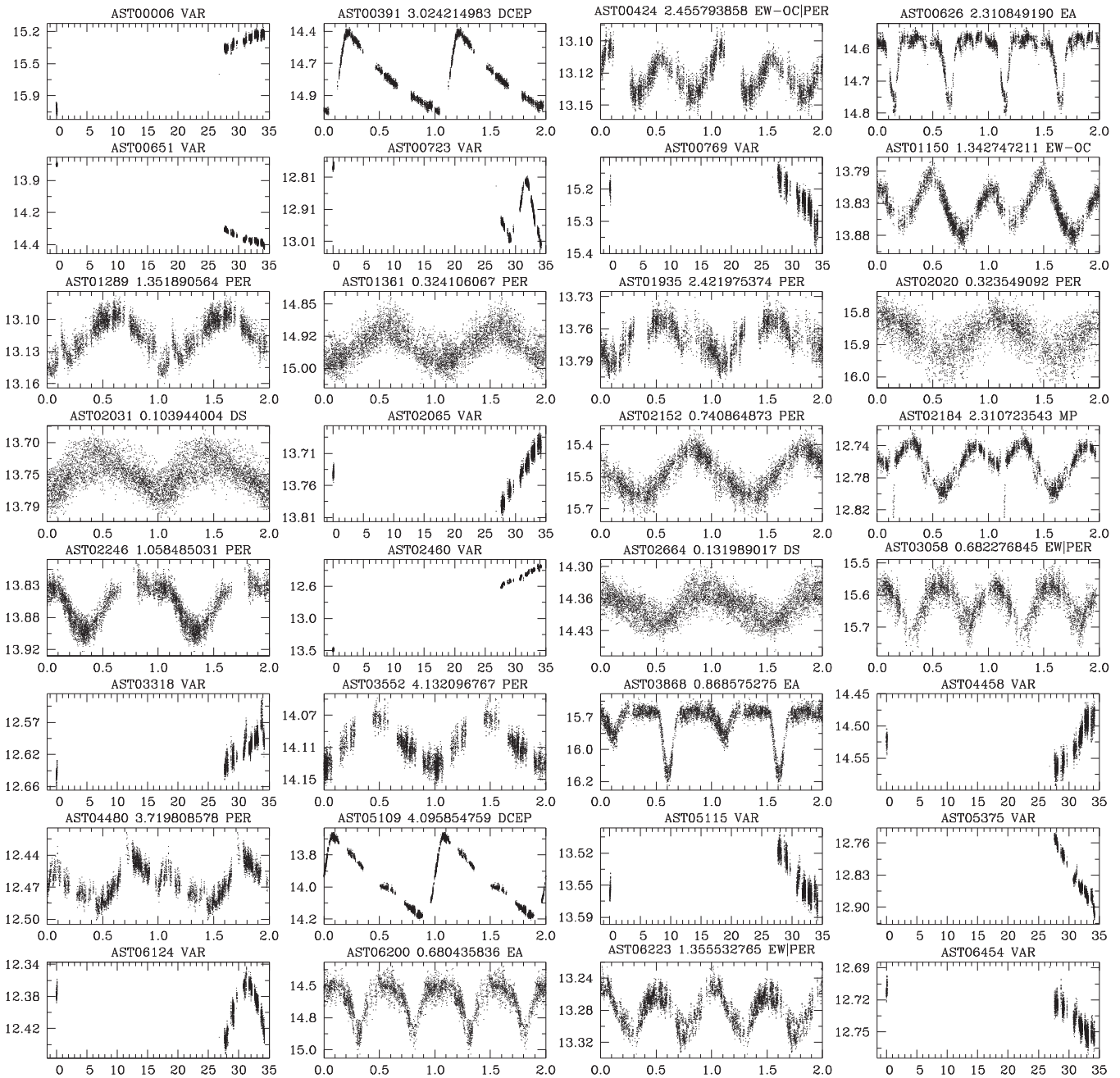


Figure 10. Phase diagram when the period is available, or the time-series plot since 2012 March 28 (JD–2456015.3164) for the 339 newly detected variables after applying 3σ outlier rejection to the measurements.

survey strategy can be found in Ma et al. (2012), Shang et al. (2012), Z. Shang et al. (2016, in preparation), and Q. Liu et al. (2016, in preparation). Of the total of 3523 images obtained of our field, 65% had exposure times of 30 s, and the remainder were 60 s. The field is not crowded as the median distance between every star and its nearest neighbor from our reference frame is 11.14 pixels (note that the AST3-1 pixel scale is 1.0 arcseconds/pixel). The stellar brightness profiles had a median FWHM of 3.73 pixels. The low level of crowding let us use aperture photometry rather than point-spread function (PSF)-fitting.

The field probes the Galactic disk center at $l = 289^\circ 6347$, $b = -1^\circ 5718$, which was also monitored by the Optical Gravitational Lensing Experiment (OGLE-III; Figure 1 of

Pietrukowicz et al. 2013). Limited data bandwidth (128 kbps for our Iridium OpenPort system; Xu 2012) from Dome A meant that the raw images were carried back from Dome A on hard disk drives by the 29th Chinese Antarctic Research Expedition (CHINARE) team. The satellite bandwidth is sufficient for transferring only small sections of images and highly reduced data (Shang et al. 2012).

2.2. Data Reduction

The preliminary reduction of the raw science images involved crosstalk correction, bias subtraction, dark current subtraction, and flat fielding. The interchannel interference crosstalk caused by the

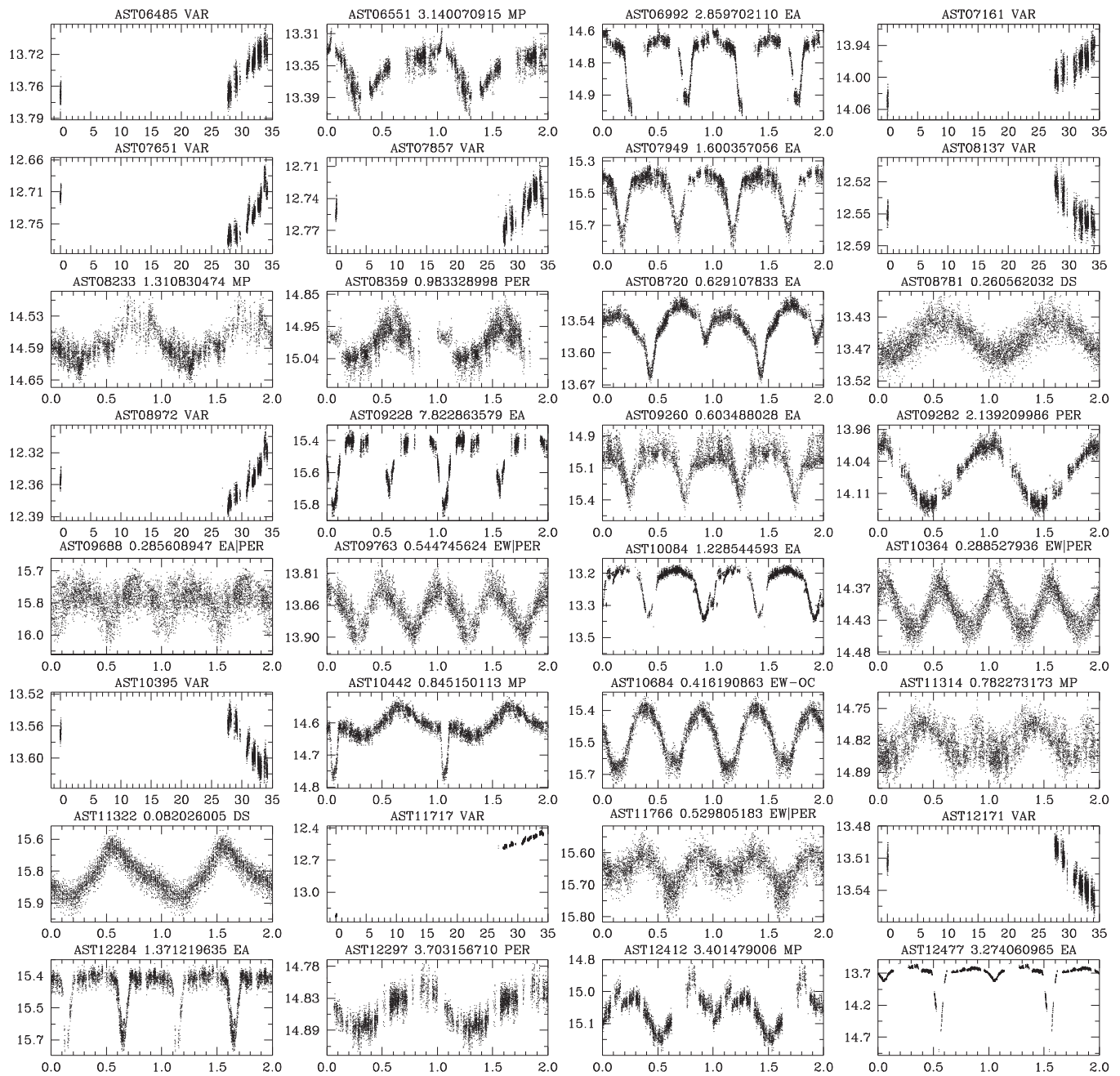


Figure 10. (Continued.)

multichannel CCD readout was corrected first. Overscan regions of the 16 readouts were used to correct the corresponding bias. Problems with the CCD thermoelectric cooler during 2012 meant that the images were subject to high dark current levels, comparable to the sky background. A new method was applied to calculate a dark frame from image pairs. More specifically, our dark frame was derived by combining 230 image pairs (each pair having the same temperature and exposure time), and was scaled to the same temperature and exposure time as the scientific images for dark current correction (Ma et al. 2014).

The flat-fielding of the AST3-1 wide field was achieved in two steps. Owing to the relatively large 4.3 deg^2 FOV, a sky brightness gradient of $1\% \sim 10\%$ from individual twilight

flat-field images remained after preprocessing for crosstalk, overscan, and dark current. The 200 twilight flat-field images were selected to correct the sky brightness gradient. More specifically, for each of the 200 twilight flat-field images, the brightness gradient was first fitted with an empirical function based on the Sun's altitude and on the angle between the image and the Sun. The gradient was removed by dividing each image by the empirical fit, and the resulting 200 twilight images were then median-combined to obtain a master flat field, which was used for flat-fielding corrections for the science images (Wei et al. 2014).

After finishing the preliminary reduction, SExtractor (Bertin & Arnouts 1996) was applied to perform aperture photometry

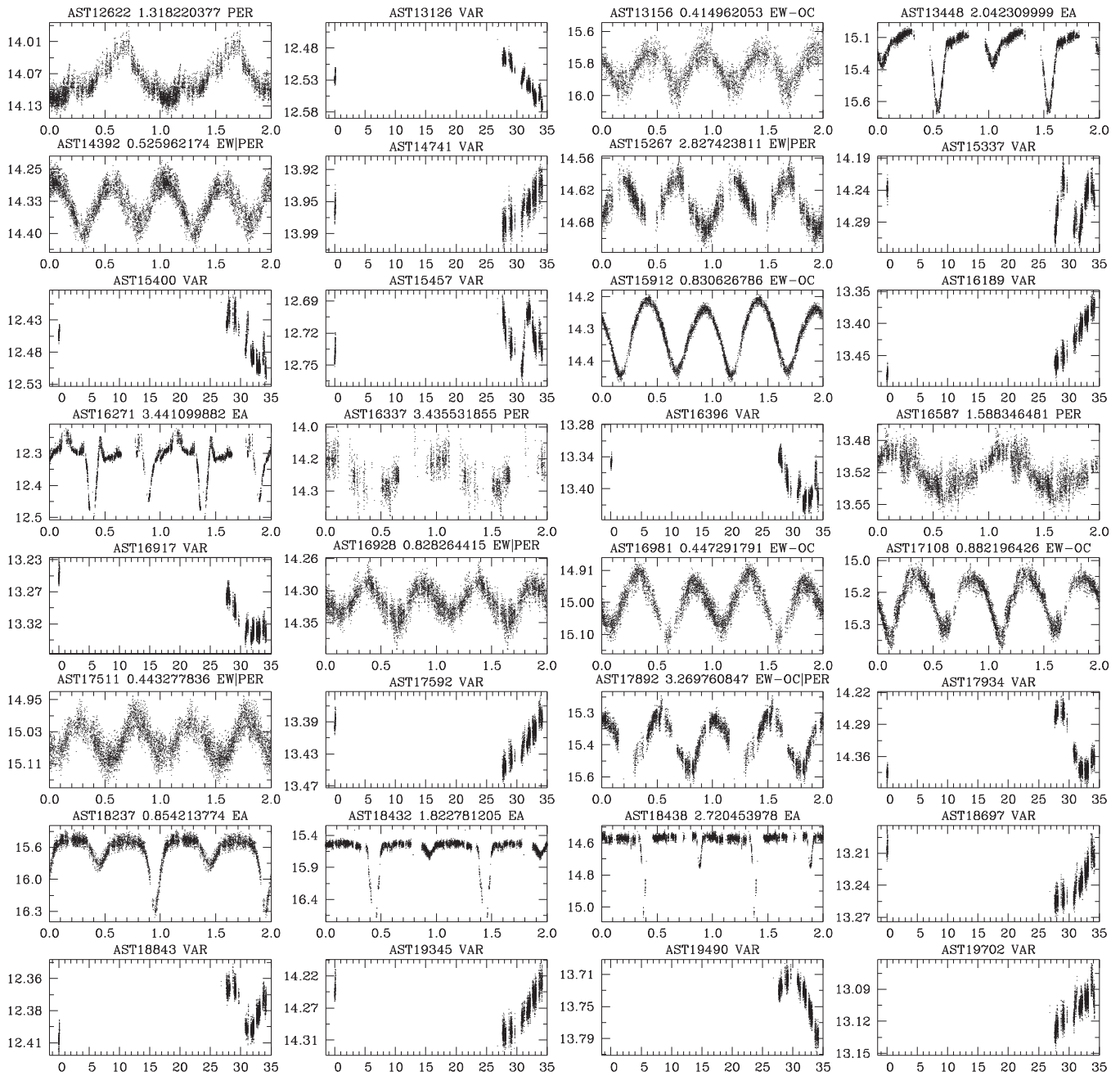


Figure 10. (Continued.)

on all the scientific images. The aperture selection with four pixels (SExtractor's `MAG_APER` parameter) was adopted as it gave the minimum rms photometric uncertainties on a test image (B. Ma et al. 2016, in preparation). The photometric uncertainty reached 2 mmag for bright stars <13 mag on a typical image. In order to obtain accurate astrometry, the photometric results were fed into SCAMP (Bertin 2006) to register the positions of all the images with the PPMX system (Position and Proper Motions eXtended, Röser et al. 2008). Our photometric calibration was divided into two steps. First, a magnitude difference between an individual image and the reference image (the highest quality image) was obtained by matching ~ 1000 bright isolated stars. Then, stars in the reference image that were also in the APASS (the AAVSO

Photometric All-Sky Survey¹⁵) catalog (Henden et al. 2016) were used to adjust the zero-point of our magnitudes. APASS is an all-sky photometric survey that is conducted in five filters: Johnson B and V, plus Sloan g , r , i bands. The AAVSO (American Association of Variable Star Observer¹⁶) was created by amateur astronomers and collects and archives variable star observations.

2.3. Time-series Photometry

During the eight days of observations, 3523 images were collected in total for our field and 96,734 bright stars with

¹⁵ <https://www.aavso.org/apass>

¹⁶ <https://www.aavso.org/>

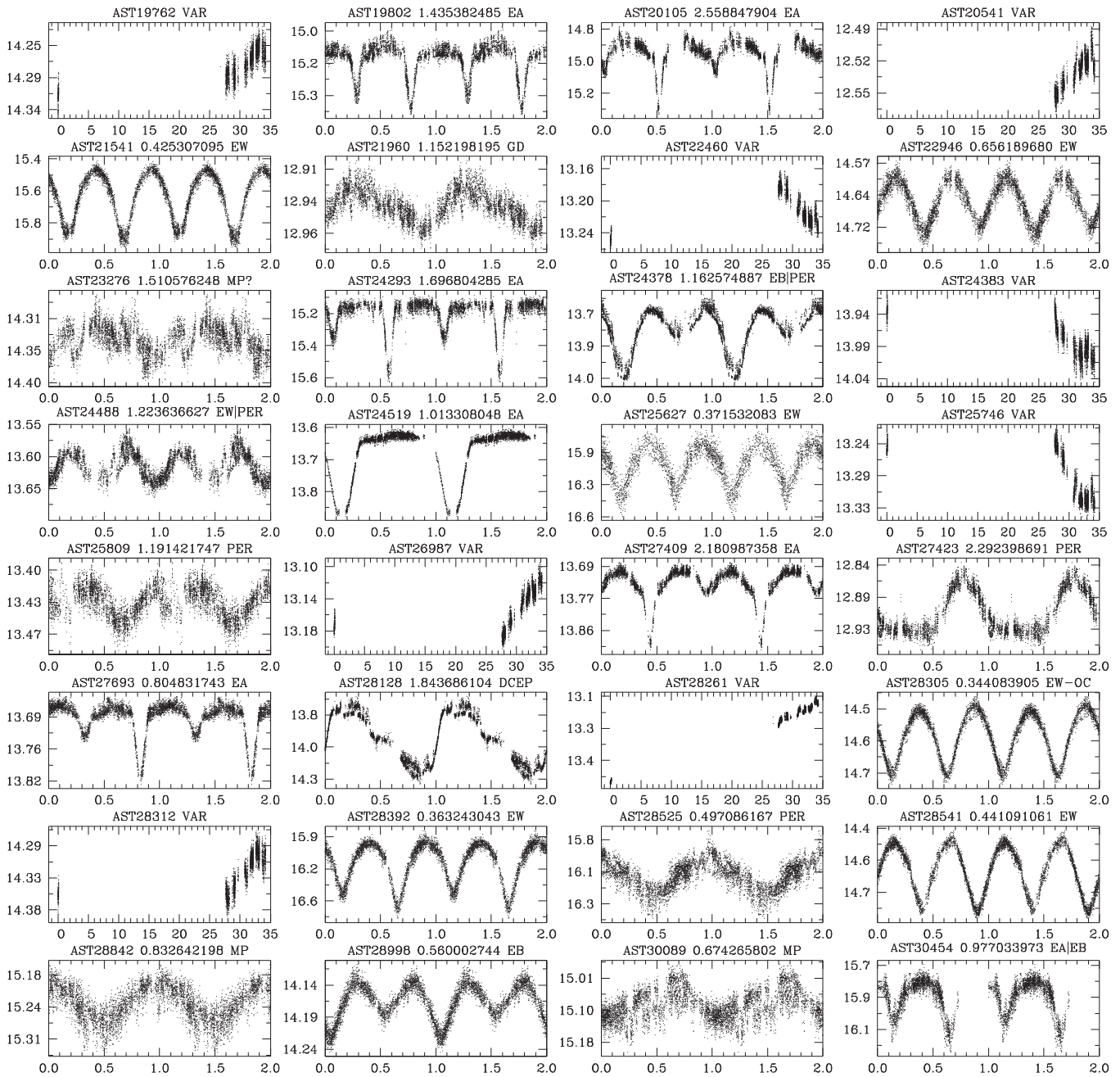


Figure 10. (Continued.)

$S/N > 30$ were found on our reference image, which had the largest number of detections. We then rejected stars that were detected in fewer than 20% of the images. We ignored these objects, but they might be interesting. This left a final sample of 92,583 stars.

Figure 1 displays the rms variations in the light curves of our sample stars as a function of error-weighted magnitude. The magnitudes were weighted by their photometric errors after rejecting 3σ outliers iteratively until the maximum iteration reached 10. The rms is lower than 0.02 mag for stars brighter than 15.4 mag. The rms is lower than 0.05 mag when the magnitudes are smaller than 16.4 mag, which accounts for 78% stars in our sample.

The photometric errors estimated by SExtractor VAR were underestimated for various reasons such as underestimated flat-fielding errors, and less than perfect photometry. We worked around this problem by assuming that the majority of stars are constant and assuming that the errors for this majority are roughly Gaussian as the $\chi^2/N_{\text{DOF}} = 1$ for the constant stars. Following the reference in Kaluzny et al. (1998), we first calculated the χ^2/N_{DOF} value for all the stars and then derived a scale factor curve for constant stars. Then we rescaled all stars by multiplying by this curve. The rescaled photometric errors were then used in the calculation of the Welch–Stetson variability index L (Welch & Stetson 1993; Stetson 1996) to find variable candidates for the next section.

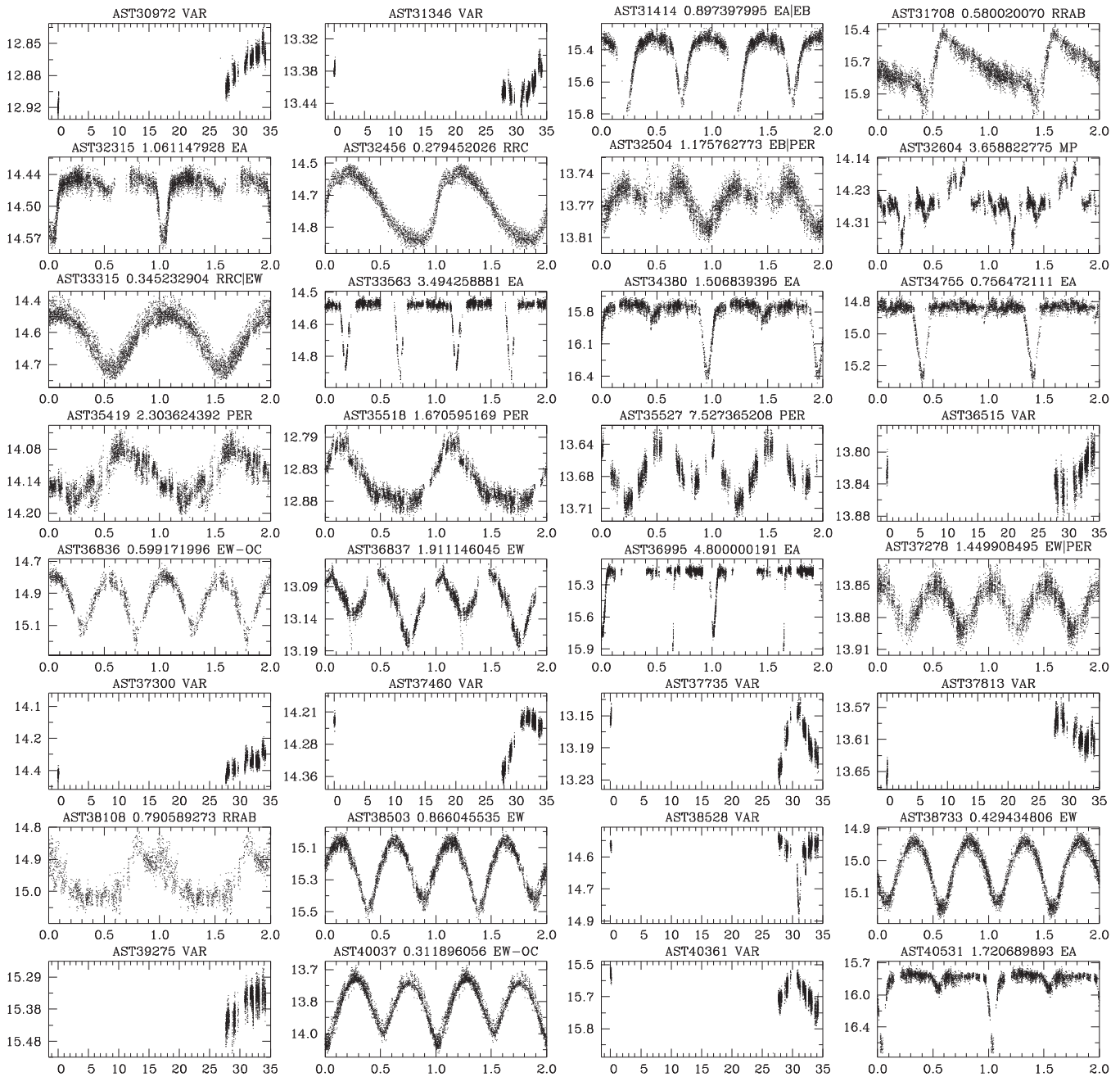


Figure 10. (Continued.)

3. Variable Star Catalog and Statistics

3.1. Searching for Variability

The search for variable stars in our sample was conducted in three steps. Our candidates were initially selected as stars with statistically significant magnitude variations. These stars did not necessarily show a periodic behavior. For the selected candidates we then conducted a search for periodic behavior. Finally, we used visual inspection of the phase-folded light curve and time-series diagram of each candidate to distinguish periodic and aperiodic variables.

Variable stars exhibit magnitude variations that can be measured by the Welch–Stetson index (Welch & Stetson 1993), which has later been slightly modified as the L variability index

by Stetson (1996). We calculated L for each light curve in our sample using VARTOOLS¹⁷ (Hartman et al. 2008; Hartman & Bakos 2016). The resulting L distribution in our sample is shown in Figure 2; the overall distribution can be interpreted in terms of two components, one of which—the component that presumably corresponds to non-variable stars—resembles a Gaussian, while the other component—presumably corresponding to the variables—behaves rather like an exponential tail. We measured a median value of $L = 0.22 \pm 0.17$ for all stars with $L < 0.8$. We used $L \geq 0.65$ (equivalent to a $+2.5\sigma$ selection) as the cutoff for our variable candidates.

¹⁷ <http://www.astro.princeton.edu/~jhartman/vartools.html>

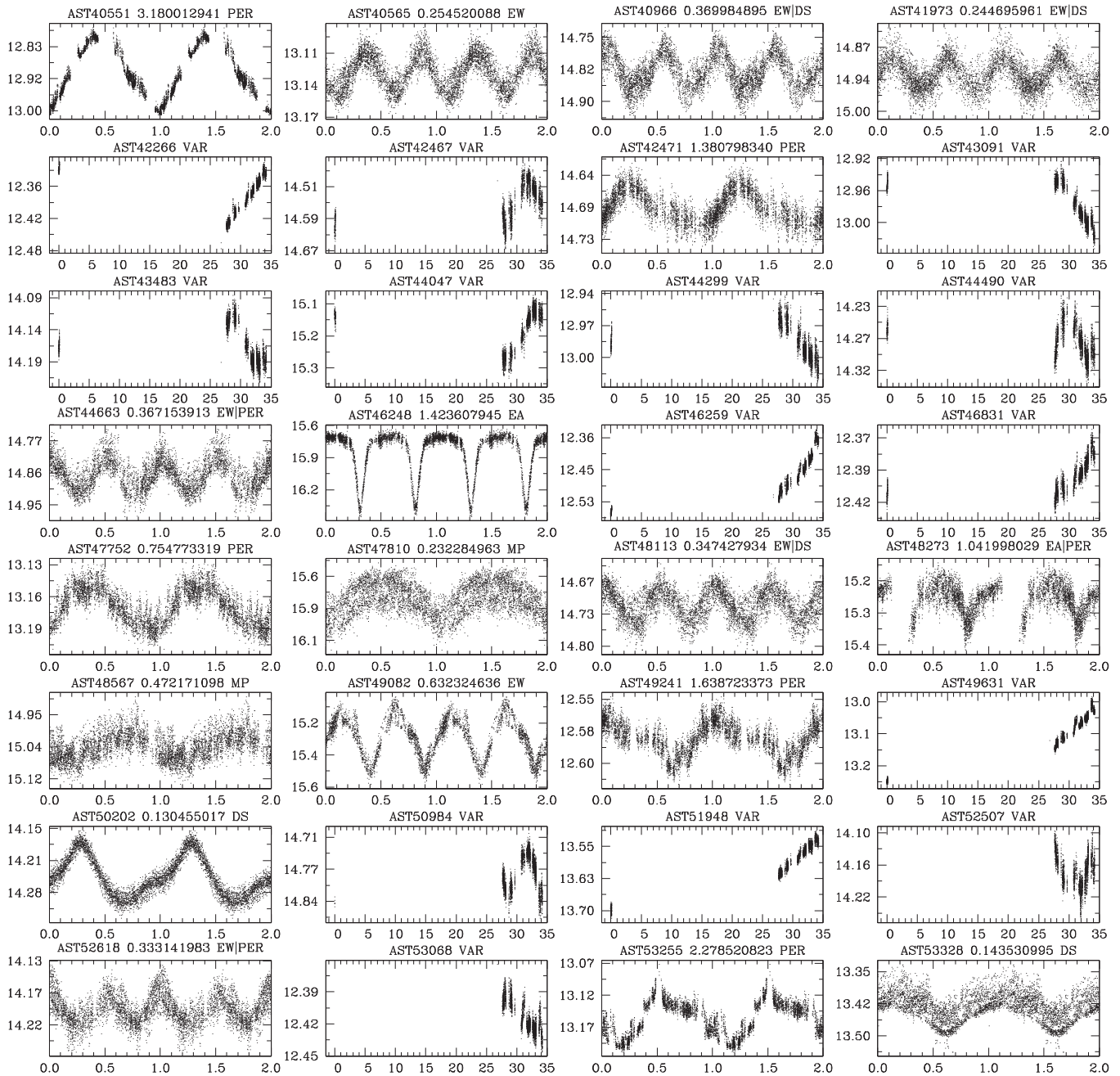


Figure 10. (Continued.)

We use Lomb–Scargle (Lomb 1976; Scargle 1982, hereinafter LS) and box fitting algorithms (Kovács et al. 2002, hereinafter BLS) to detect the periods of our variable candidates. The LS method applies the statistical properties of least-squares frequency analysis of unequally spaced data on a series of test periods. We hunted for periods between 0.01 and 10 days and applied a bin size of 0.01 days. Periods with $S/N \geq 12$ in the periodogram were taken to be significant. The BLS method searches for signals characterized by a periodic alternation between two discrete levels with much less time spent at the low-level (occultation) phase. Similar methods (LS and BLS) for hunting for variable stars were applied in Wang

et al. (2011, 2013a) and Yao et al. (2015). Surveys such as OGLE II use the detached eclipsing binary light-curve fitter (Devor 2005, hereinafter DEBiL) for finding and analyzing eclipsing binaries in large data sets. We also used the DEBiL code to find the corresponding periods of our variable candidates as an independent check of the periods found by the LS and BLS methods. We visually inspected the phased light curve folded by the periods found from each of the LS, BLS, and DEBiL methods, and selected the period that had the smallest rms. Because of the very short observing window (only 8 days of observations in 34 days) and observing gaps (when AST-3 was pointing elsewhere, and avoiding twilight),

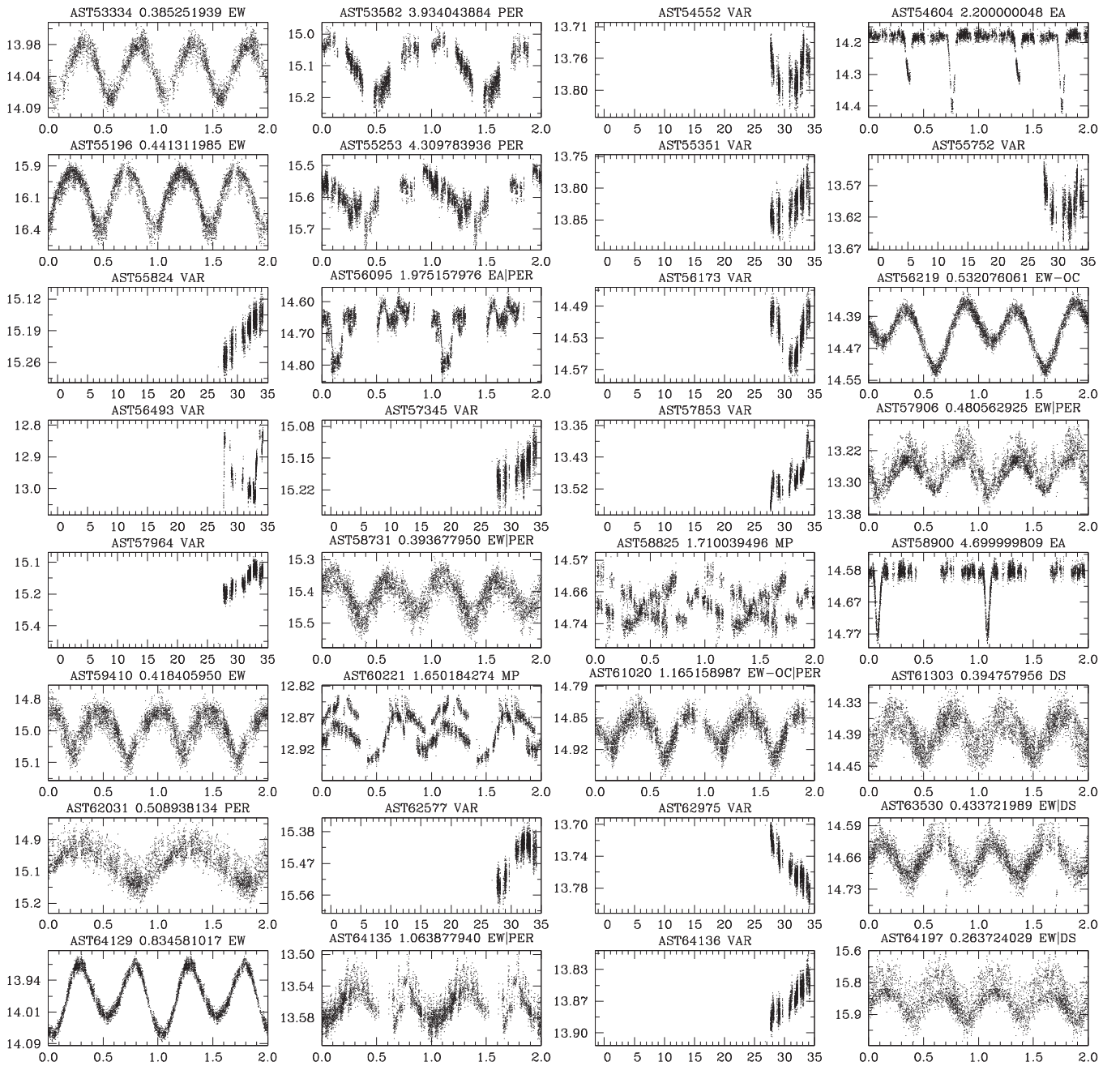


Figure 10. (Continued.)

we found that in some cases periods produced by the LS, BLS, or DEBIl methods did not produce well-folded phase curves. In these cases, we manually adjusted the period to produce the best result.

In order to calculate the uncertainty of the above derived periods, we ran Markov chain Monte Carlo (MCMC; Brooks 1998) simulations of the high-order harmonic function as given in Equation (1),

$$F(t) = a_0 + \sum_{i=1}^{12} \left[a_i \sin\left(\frac{2\pi ti}{P}\right) + b_i \cos\left(\frac{2\pi ti}{P}\right) \right], \quad (1)$$

based on the detected period using the *-nonlinfit* tool of VARTOOLS (Hartman & Bakos 2016). We used a 12th order

fit to the light curve, which was able to fit eclipsing binaries with relative deep depths. The number of accepted links in a given fit was set to 1000. The initial guess and step size of each a_i and b_i were found by fitting the Equation (1) to each light curve with a fixed period. The median value of each period and its uncertainty were calculated in the MCMC simulation by again fitting the Equation (1) to each light curve, but now with the constraint $0.01 < P < 8.0$.

Next, we visually inspected the light curve of each variable candidate to search for objects with statistically significant variations in magnitude that did not necessarily show a periodic behavior during our eight observation days. Our final catalog of variables contains 560 stars in the magnitude range from

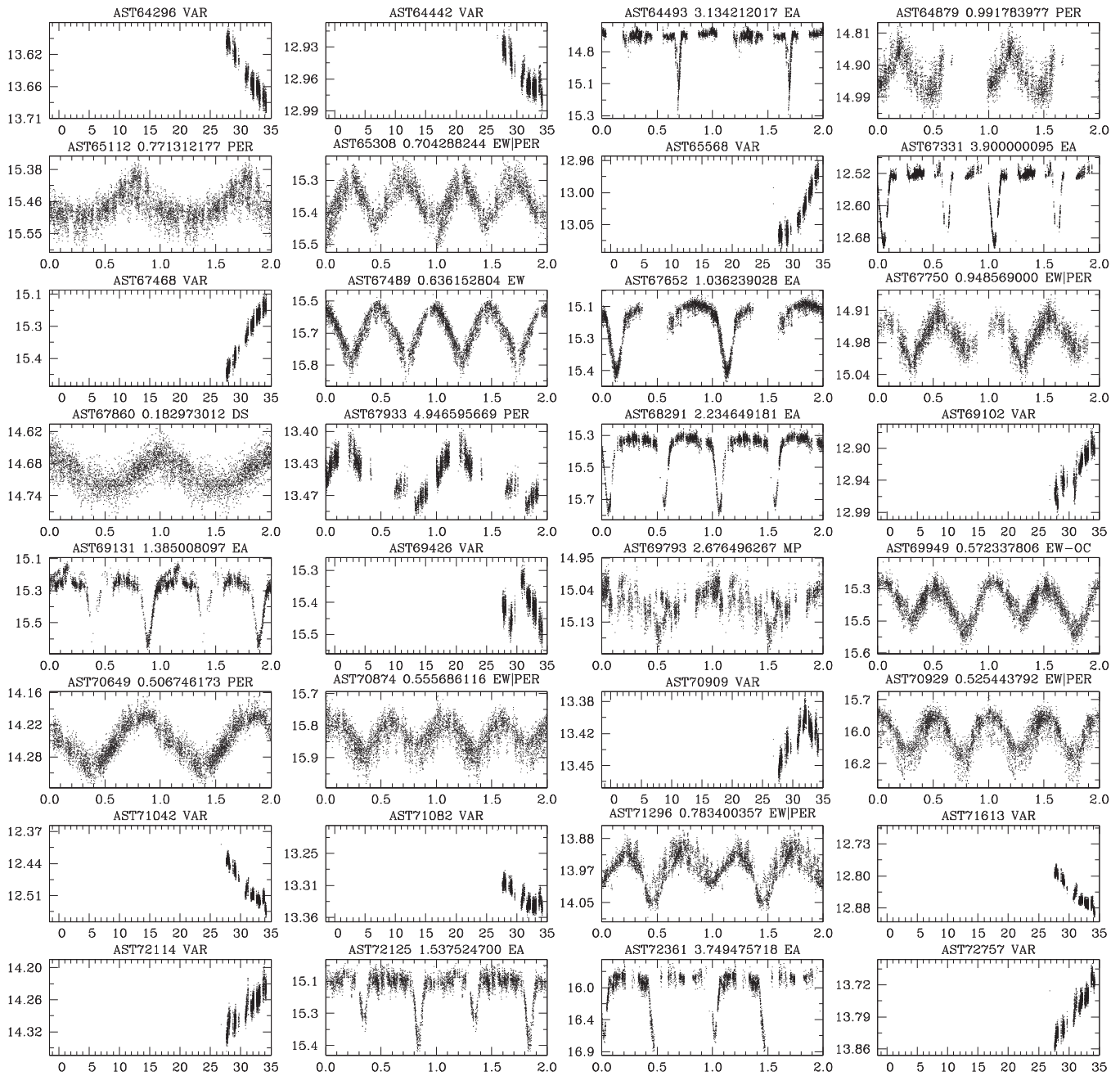


Figure 10. (Continued.)

10.87 mag to 16.23 mag, 339 of which are new discoveries by AST3-1. Table 2 lists the properties of all the detected variables. Column 1 lists the 2012 AST3 ID; columns 2 and 3 give the right ascension and declination matched to the PPMX system; column 4 contains the weighted mean i -band magnitude; column 5 gives the L value; column 6 lists the most significant median period (top left panel in Figure 3) in the MCMC simulation and its standard deviation in brackets in units of 10^{-9} days (when applicable); column 7 specifies the minimum χ^2 per degree of freedom in the MCMC simulation; column 8 gives the peak-to-peak amplitude of variation; column 9 gives the time of the first minimum light contained in our observations (only for the periodic variables); column 10 contains a tentative classification of the variable,¹⁸ where

¹⁸ <http://www.sai.msu.su/groups/cluster/gcvs/gcvs/iii/vartype.txt>

possible; column 11 has additional information, including previous identification of the variable from the all-sky automated survey run by AAVSO (Pojmanski 2005; Watson et al. 2016) or inclusion in the variable stars of OGLE-III (Samus et al. 2009) or the Bochum Survey of the Southern Galactic Disk (Hackstein et al. 2015, hereinafter GDS).

We matched our final catalog of 560 stars with the AAVSO database and GDS catalog with a matching radius of 15 arcseconds. This initially resulted in 231 variable stars that were known previously. There were 116 variable stars in common between our survey and the AAVSO database, and 104 of these had magnitudes in the Cousins' infrared I_c band (Watson et al. 2016). There are 152 variable stars in common in our catalog and the GDS database with magnitude values in Sloan r band; 139 of these also had magnitude measurements in Sloan i band (Hackstein et al. 2015), which is similar to our

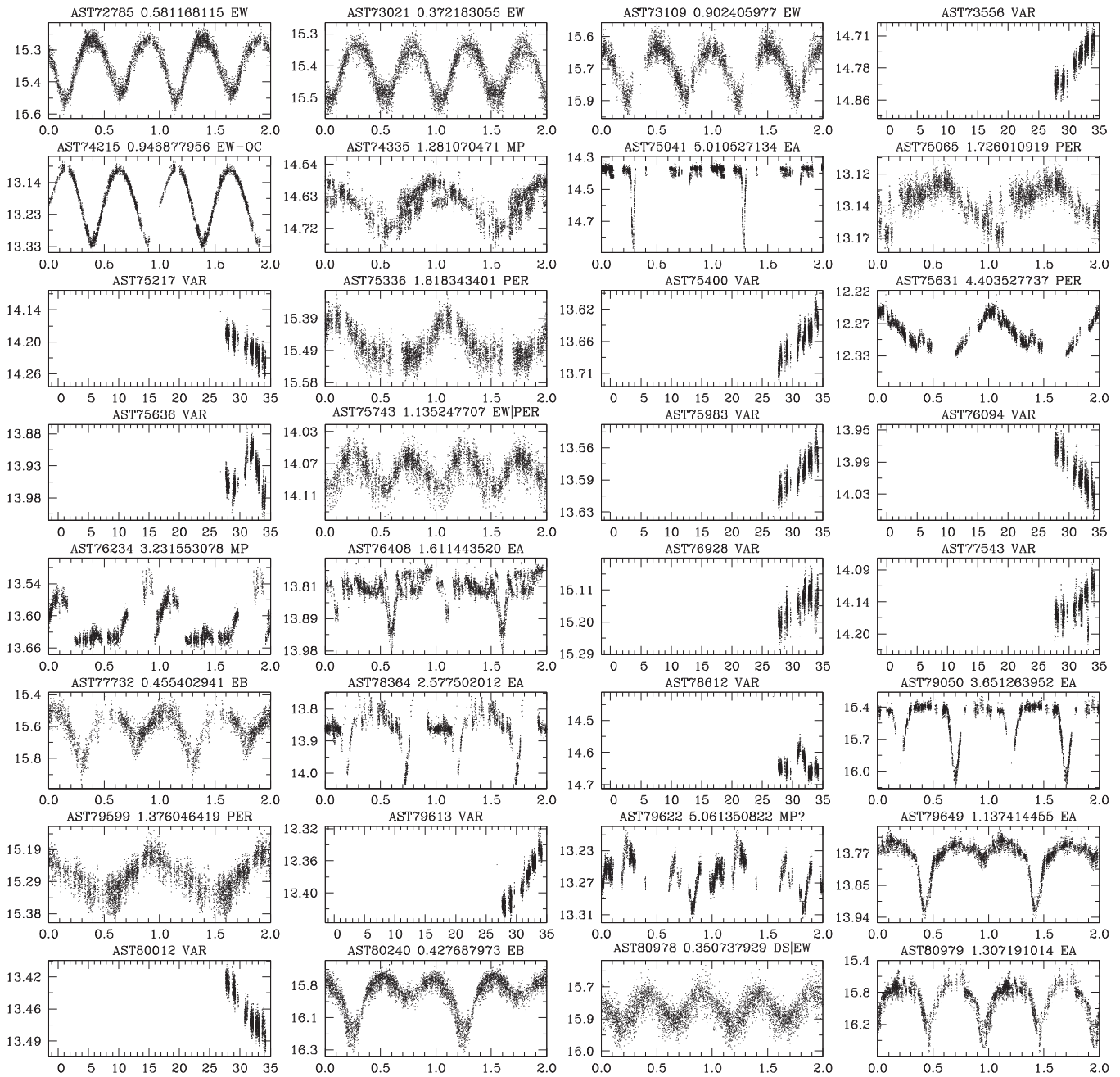


Figure 10. (Continued.)

filter. Thirty-seven variables appeared in both the AAVSO database and the GDS catalog. We double-checked our initial matching results by measuring the magnitude difference Δmag of our observations and I_c (AAVSO) and i (GDS). For the 104 stars in common with the AAVSO database, we measured a median value of $\Delta \text{mag} = (i - I_c) = 0.553 \pm 0.316$ and applied a 3σ outlier rejection to the Δmag and also required that the I_c magnitude should be lower than 16.5 mag to exclude 6 stars (AST11766, 12622, 37735, 64879, 74215, and 89418) from the initial common sample. The i versus I_c magnitude diagram for the remaining 98 variable stars is shown in the right panel of Figure 3. We excluded 4 outliers (AST05375,

57964, 71042, and 83522) with the same method applied to the 139 stars in common between our catalog and GDS. i versus r for 148 variables we have in common with GDS is shown in the bottom left panel of Figure 3; i versus i for 135 variables is shown in the bottom right panel.

Our final catalog shows that we have rediscovered 221 previously known variable stars; 96 of these are found in both the AAVSO database and the OGLE-III survey (Pietrukowicz et al. 2013); an additional 14 stars were in the AAVSO database but not in the OGLE-III survey; the remaining 111 stars were found in the GDS catalog. Because of our short observing window, we could not determine the periods of three variables:

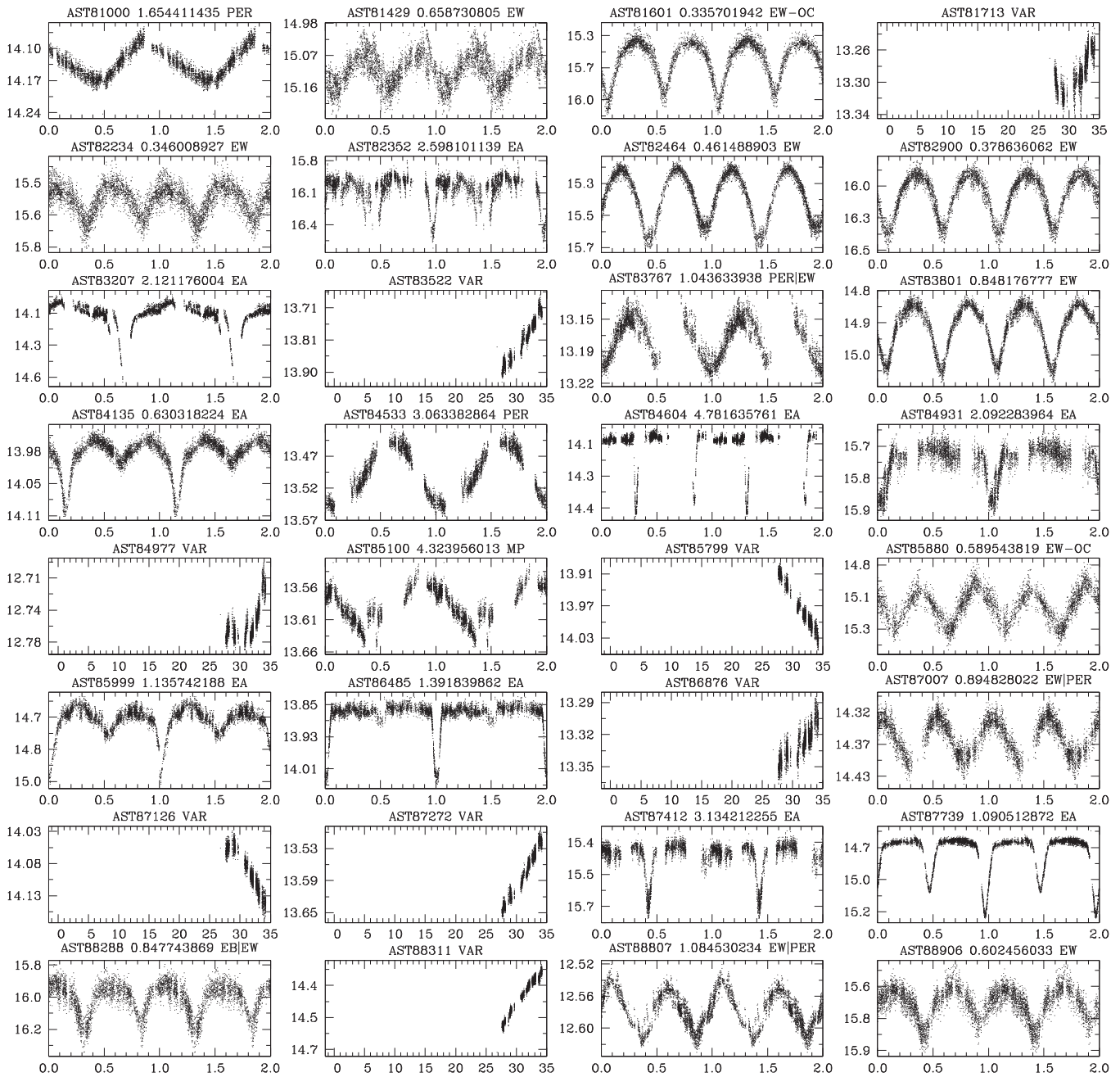


Figure 10. (Continued.)

AST13431, 49035, and 83717. In addition, AST43064 and 62877 are listed in the AAVSO database without a period, and none of the known variables from the GDS catalog had measurements of their periods until now. The estimated periods for the remaining 105 variables from AST3-1 are highly consistent with those given in the AAVSO database except for five variables: AST31492, 38531, 39901, 59773, and 68860, which have AST3-1 periods that are half of the AAVSO values. Our period detection methods (LS and BLS) are sensitive to detecting sine wave or box-like signals. Our periods should be double for binary stars to show the primary and secondary eclipsing light variabilities, i.e., binaries AST38531, 59773, and 68860, while for another two periodic variable stars, AST31492 and 39901, our periods are probably

correct (Figure 4). The final period-period diagram from the AST3-1 and AAVSO database is shown in the top left panel of Figure 3.

We classified half of the variables into binaries, 17% of them into δ Scuti, γ Doradus, δ Cephei, RR Lyrae, and unclassified periodic or multiple periodic variables. Because of our short observing window, we could not detect the periods of the one-third of the variables that passed our selection as a result of their significant time-series variability. Table 3 contains approximate statistics for the different types, when possible. The folded light curves of the representative periodic variables are shown in Figures 5–8, while the representative light curves of aperiodic variables are shown in

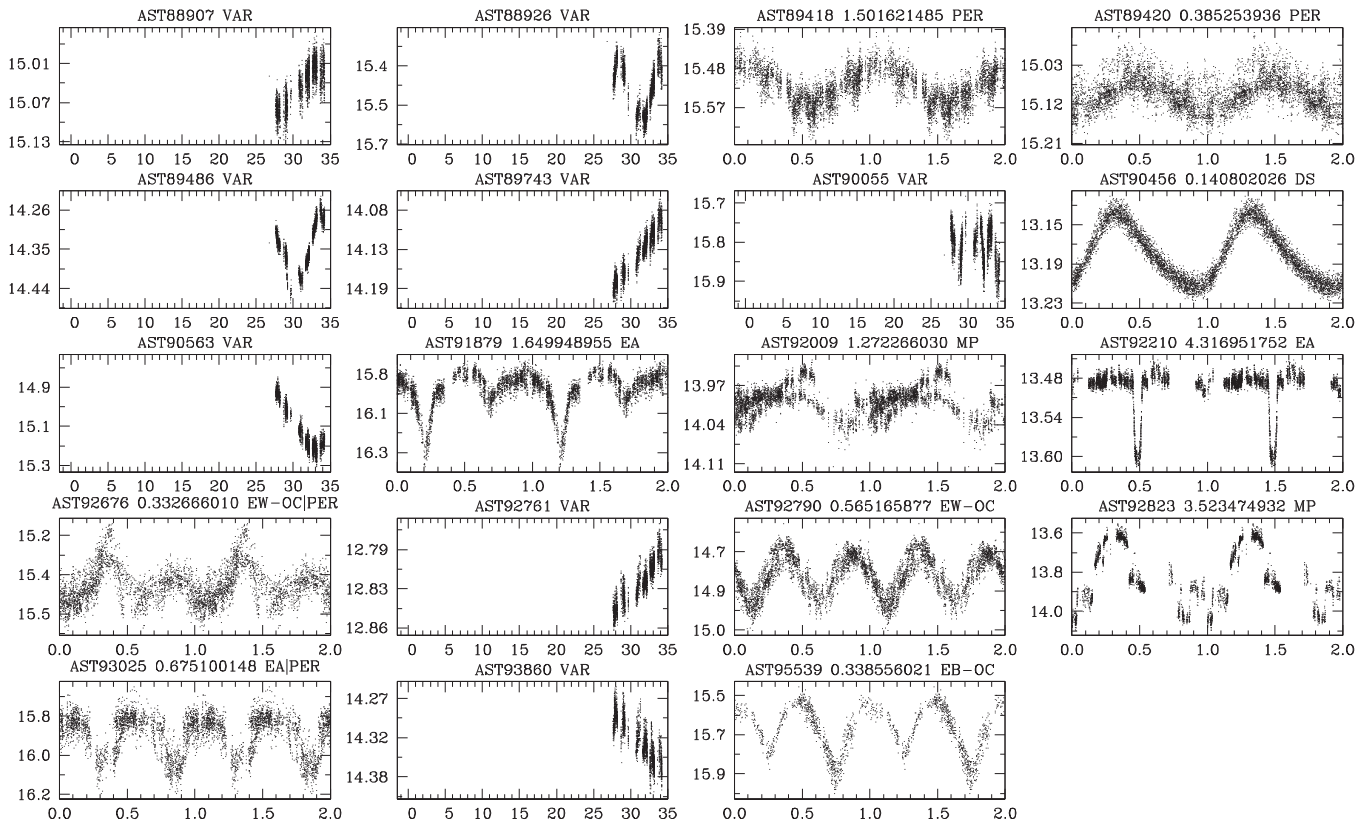


Figure 10. (Continued.)

Figure 9. All phased or time-series light curves of the 339 newly detected variables are shown in the appendix in Figure 10, and the same figures for the 221 previously known variable stars in Table 4 are displayed in Figure 11. The time-series data of all 560 variable stars will be available in machine readable format in the online Journal and through the VizieR Online Data Catalog.¹⁹

3.2. Types of Variables Found by AST3-1

3.2.1. Eclipsing Binaries

Eclipsing binaries can be classified into three broad categories based on the shape of their light curves: Algol-type eclipsing systems (EAs), β Lyrae-type eclipsing systems (EBs), and W Ursae Majoris-type eclipsing variables (EWs). The EA systems have obviously different depths between the primary and secondary minima, and have clearly defined times for the beginning and end of the eclipses; EA systems are often but not always a detached eclipsing system (Catelan & Smith 2015), although the prototype of the class, Algol, is believed to be a semi-detached system (Soderhjelm 1980; Kolbas et al. 2015). The EB systems show a continuous change in brightness and have a deeper primary depth than that of the secondary. The EW systems also show a continuous change in brightness and have an almost equal or non-obvious varying depth between the primary and secondary minima. The EW systems consist of two components that are almost in contact and thus have periods generally shorter than one day. There are 127 EWs, 33 EBs, and 138 EAs in our sample, and 65 stars in question are

probably distributed into several different variability classes, including eclipsers, pulsators, and others, which are separated by a pipe symbol “|” in Table 2. In total, we have detected 285 binaries, 143 of which are new detections from our data. Of the 339 new variables, 42% belong to the classes of eclipsing binary stars.

There are 34 interesting EW or EB binaries in our 285 detections that show O’Connell effects, i.e., the two successive out-of-eclipse maxima have unequal height in the light curves (O’Connell 1951; Milone 1968; Nataf et al. 2010). The O’Connell effect can be explained by the interaction of circumstellar material with the binary components (Liu & Yang 2003). The interaction model suggests that the O’Connell effect is most obvious in late-type and/or short-period binaries. In our sample, a short-period EW binary AST46538 exhibits the most obvious O’Connell effect (Figure 6) and has a magnitude difference of 0.06 mag in i band between the first and second maximum out-of-eclipse brightness. AST46538 appears in the UCAC4 catalog (Fourth U.S. Naval Observatory CCD Astrograph Catalog; Zacharias et al. 2013) and has $B = 13.697$ mag and $V = 12.916$ mag. It also appears in the 2MASS All-Sky catalog of Point Sources (Cutri et al. 2003) and has J , H , K of 11.311 ± 0.026 , 10.941 ± 0.029 , 10.842 ± 0.027 mag., respectively. In order to estimate the color excess $E(B - V)$ of AST46538, we compared its color-color diagrams ($V - J$ versus $B - V$, $V - H$ versus $B - V$, $V - K$ versus $B - V$, $J - H$ versus $B - V$ and $H - K$ versus $B - V$) with the intrinsic color-color diagrams for main-sequence stars²⁰ (Fitzgerald 1970; Ducati et al. 2001), and we found that its interstellar extinction can be neglected. Thus the color term of AST46538 from UCAC4 and

¹⁹ <http://vizier.u-strasbg.fr/>

²⁰ <http://www.stsci.edu/~inr/intrins.html>

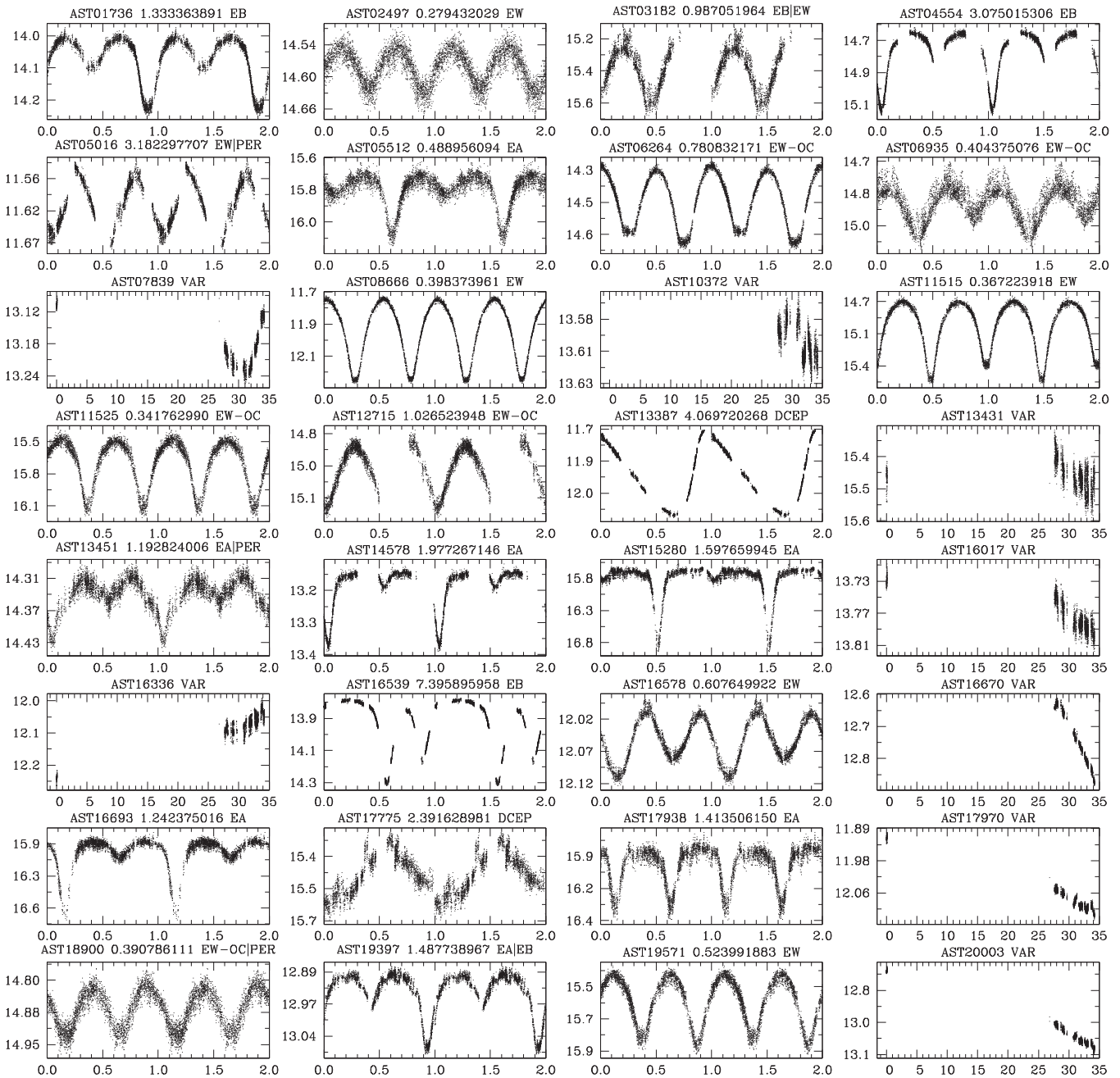


Figure 11. Phase diagram when the period is available, or the time-series plot since 2012 March 28 (JD–2456015.3164) for the 221 previously known variables after applying 3σ outlier rejection to the measurements.

2MASS catalogs can be taken as its intrinsic color to estimate its spectral type, which is equivalent to spectral type G8 (Fitzgerald 1970; Ducati et al. 2001). We find that the spectral type G8 and orbital period 0.333 days of AST46538 are close to that of the W UMa binary YY Eri with spectral type G5V and orbital period 0.322 days (Liu & Yang 2003); both should therefore exhibit similar O’Connell effects based on the model of Liu & Yang (2003). Indeed, we find consistent O’Connell effects in AST46538 and YY Eri: for YY Eri, the modeled bolometric magnitude difference is 0.07 mag and the observed magnitude difference in V band is 0.04 mag (Liu & Yang 2003), while for AST46538, the observed magnitude difference in i band is

0.06 mag. More observations are needed to double-check this analysis for AST46538.

3.2.2. Pulsating Variable Stars

Pulsating variable stars exhibit periodic expansion and contraction (radially or non-radially) of their surface layers (Catelan & Smith 2015). The pulsating variable stars are classified into many types based on their period, amplitude, light-curve shape, evolutionary status, and so on. A more complete classification for all types of pulsating variable stars (δ Scuti, γ Doradus, RR Lyrae stars, Cepheids, and so on) can be found in Catelan & Smith (2015). δ Scuti

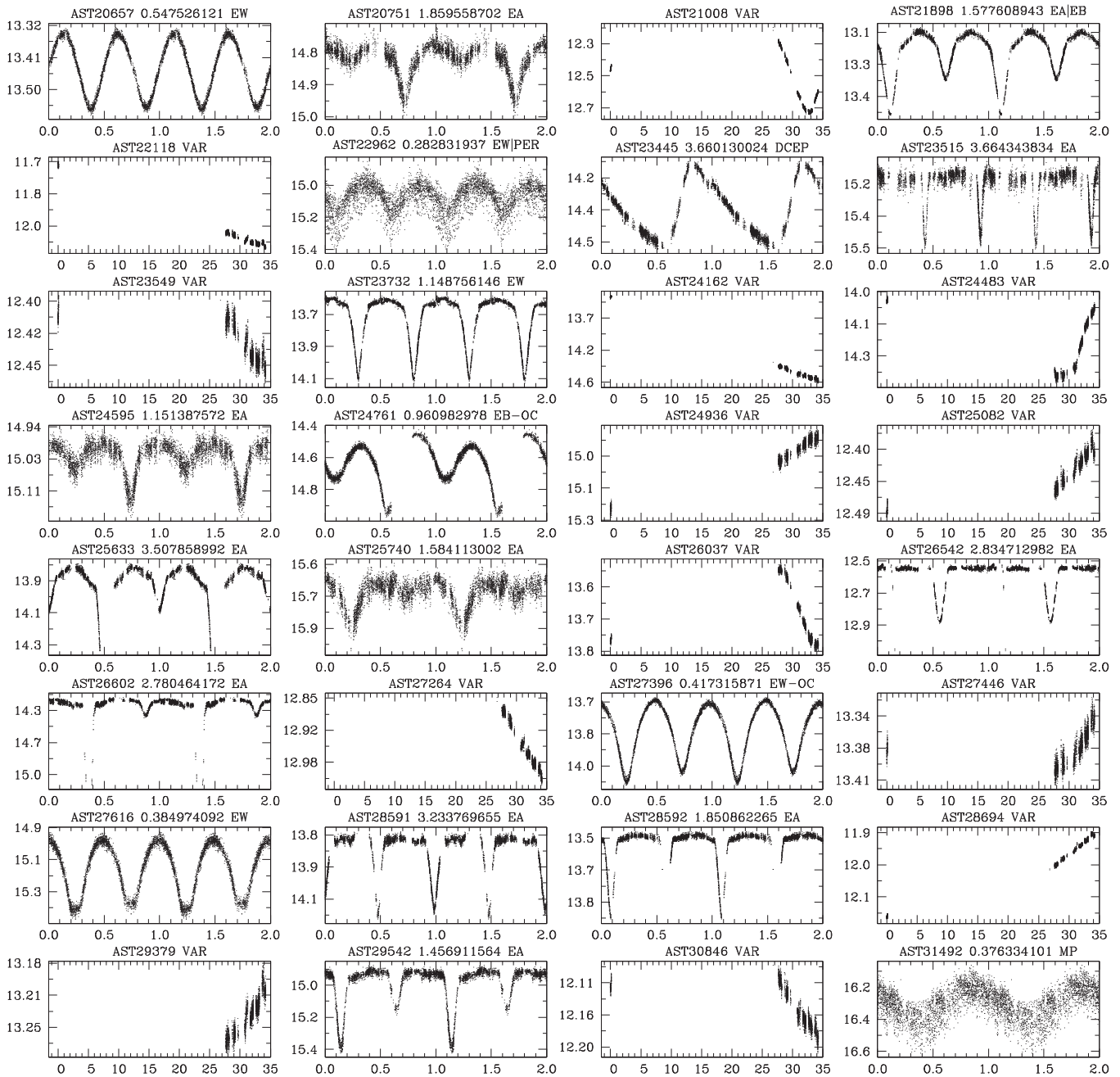


Figure 11. (Continued.)

variables are late A- and early F-type stars situated in the instability strip on or above the main sequence in the Hertzsprung-Russell diagram. Their typical pulsation periods are found to be in the range of 0.02 days to 0.25 days (Breger 2000). γ Doradus stars are located in a similar position in the instability strip as the δ Scuti stars, but with relatively longer pulsating periods of between 0.3 days to 3 days (Cuypers et al. 2009). RR Lyrae stars are radially pulsating giant stars with spectral types A to F with periods of ~ 0.2 to ~ 1 days (Smith 2004, p. 166). Most RR Lyrae stars are pulsating in the radial fundamental mode (RRab stars) and the first overtone mode (RRc stars).

Cepheid variables obey the period-luminosity relation and are divided into two subclasses—type I and type II Cepheids (Catelan & Smith 2015)—based on their masses, ages, and evolutionary

states. The period-luminosity relation shows that there is a subtype between I and II, called Anomalous Cepheids (Figure 7.3 of Catelan & Smith 2015). The majority of δ Cepheid variables show a large light variation, a rapid rise to maximum, and a slow decline back to minimum (i.e., Figure 7), which is similar to a RR Lyrae star (Schmidt et al. 2004; Soszynski et al. 2008). There are δ Cepheids with lower amplitudes (< 0.5 mag. in V), but they have symmetrical light curves and shorter periods (< 7 days; Catelan & Smith 2015). Type II Cepheids generally show a relatively broad maximum and a symmetric minimum (Schmidt et al. 2004), and they have periods of ~ 0.8 –35 days and light amplitudes from 0.3 to 1.2 mag in V band.²¹ Anomalous Cepheids show a similar light-curve morphology as RR Lyrae variables with periods

²¹ <http://www.sai.msu.su/groups/cluster/gcvs/gcvs/iii/vartype.txt>

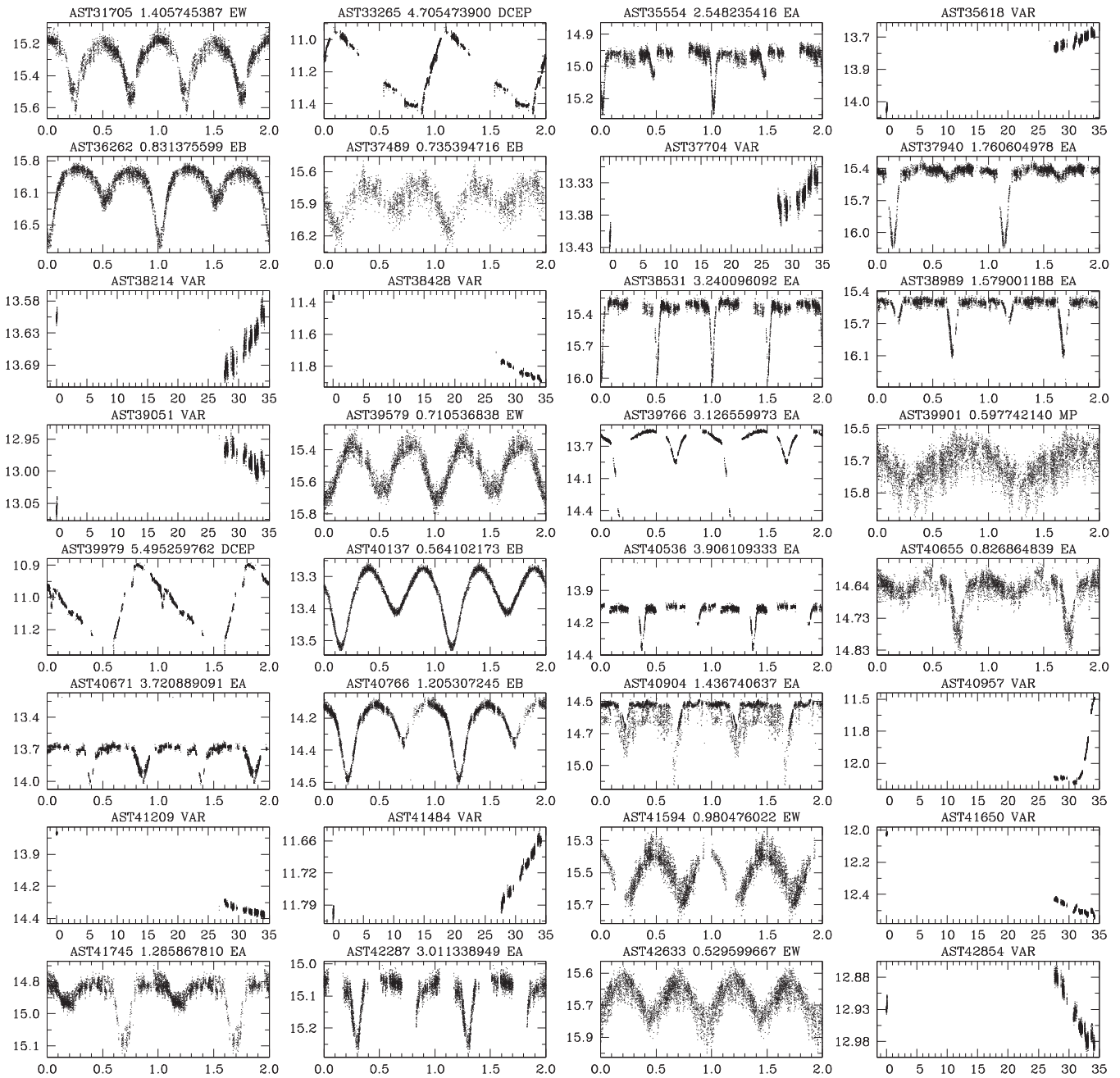


Figure 11. (Continued.)

shorter than two days, and the majority of them show a small bump before the rise to maximum (Soszyński et al. 2008). Based on the light-curve morphology, 12 variable candidates were classified as δ Cepheids as they have higher light amplitudes (>0.3 mag.), longer periods ($\gtrsim 2$ days), and also exhibit a rapid rise to maximum and a slow decline to minimum. Another 13 variables (AST04480, 09282, 35419, 35518, 40551, 42471, 49241, 53255, 67933, 75631, 79599, 81000, and 84533) also show the morphology of a fast rise and a slow fall, and we have classified them as type “PER” (Section 3.2.3) since their i amplitudes are lower than 0.3 mag. and they have no bumps before the rise to maximum.

In our sample, there are 27 pulsators, which are classified into 10 δ Scuti stars, 2 γ Doradus stars, 12 δ Cepheids, and 3

RR Lyraes. For example, AST13387 is the previously known δ Cepheid GS Car. Its phased light curve in i band can be well fitted by the Fourier decompositions with a fundamental frequency of $0.245616 \text{ days}^{-1}$ and harmonics of 0.497130 , 0.736473 , 0.984846 , and $1.225154 \text{ days}^{-1}$ in order of decreasing amplitude values (the red curves in Figure 7).

3.2.3. Other Types of Variable Stars

For 67 of the unclassified 248 variable stars we detected the main periods (periodic and multiperiodic). When the phased light curve folded by its main period was significantly scattered, we classified it as a multiperiodic-type variable star, otherwise we classified it as a periodic variable. For the remaining 181

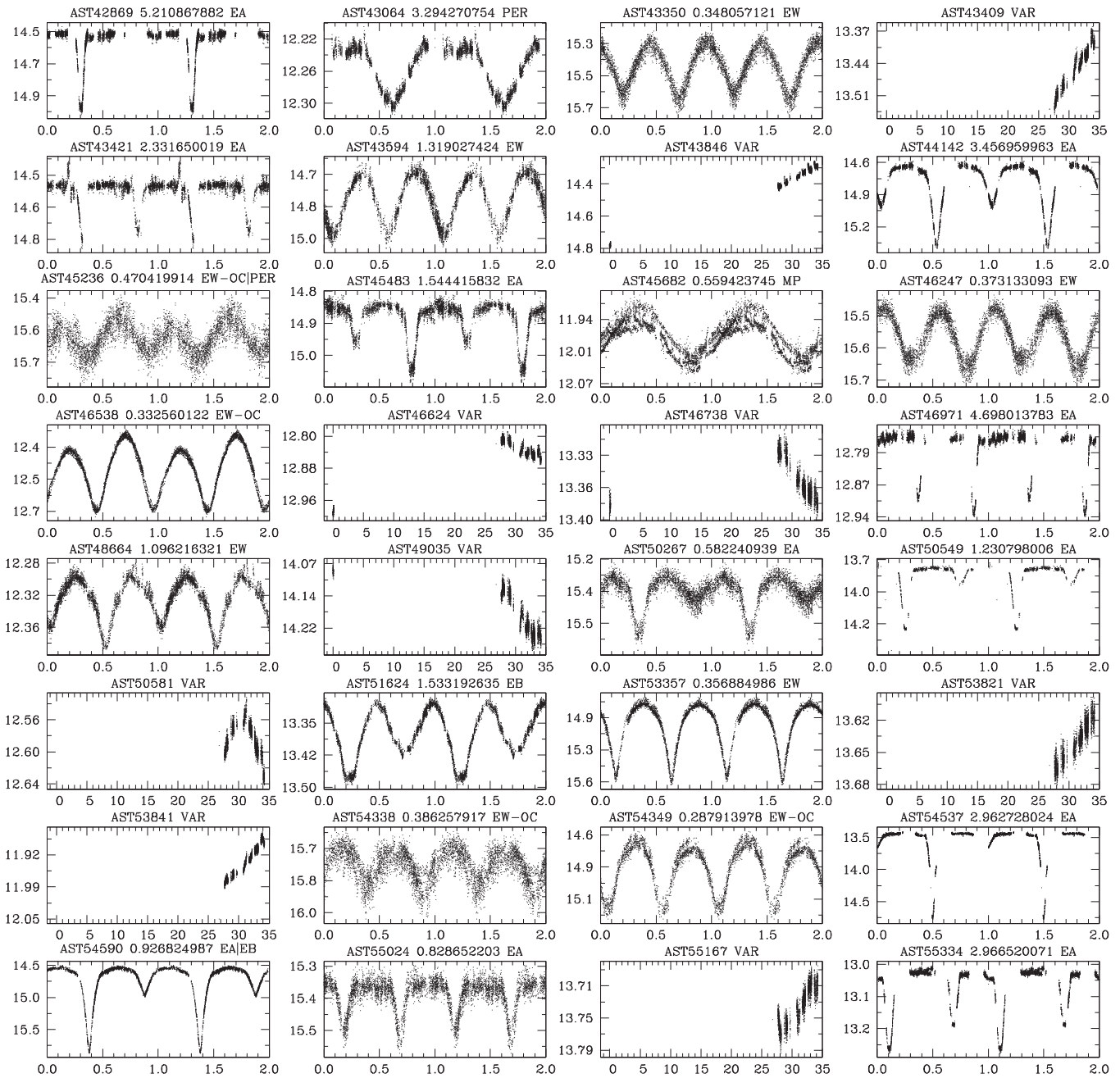


Figure 11. (Continued.)

unclassified objects we could not detect a period because of the short observing window (8 days in 34 days). In our sample, we detected a new complex binary system, AST10442 (Figure 8). The system has a period of 0.845 days and an i magnitude of 14.64. The system, which presents an RS CVn-like light-curve morphology (obvious variability when out of eclipse), shows a primary depth of 0.15 mag, but does not show the secondary eclipse in the folded light curve (bottom panel of Figure 8). AST10442 appears in the SPM4 catalog (Girard et al. 2011) and has $B = 16.59$ mag and $V = 15.24$ mag. It also appears in the 2MASS All-Sky catalog of Point Sources (Cutri et al. 2003) and has J, H, K of 13.254 ± 0.029 , 12.728 ± 0.022 , 12.548 ± 0.030 mag., respectively. We performed the same analysis (color-color diagrams) as for AST46538 and found that its

interstellar extinction can also be neglected. Based on the empirical formula $T_{\text{eff}} = \frac{8540}{(B-V)+0.865}$ (Krishna Swamy 1996; Zong et al. 2015), color $B - V = 1.35$ mag is equivalent to $T_{\text{eff}} \approx 3850$ K. Such low T_{eff} suggests that AST10442 has a spectral type of K5 or M0. If it is a giant, then its orbital velocity could be >500 km/s judging from Figure 4 of Gaulme et al. (2013). To our knowledge, no published spectroscopic observations have been performed of this interesting system to date. We have obtained 2 hr on Gemini South to carry out spectroscopic observations of this system, in order to measure its maximum radial velocities at phases 0.25 and 0.75.

In addition, out of the 181 aperiodic variable stars, four variable stars AST68688, 40957, 90095, and 83717 with the

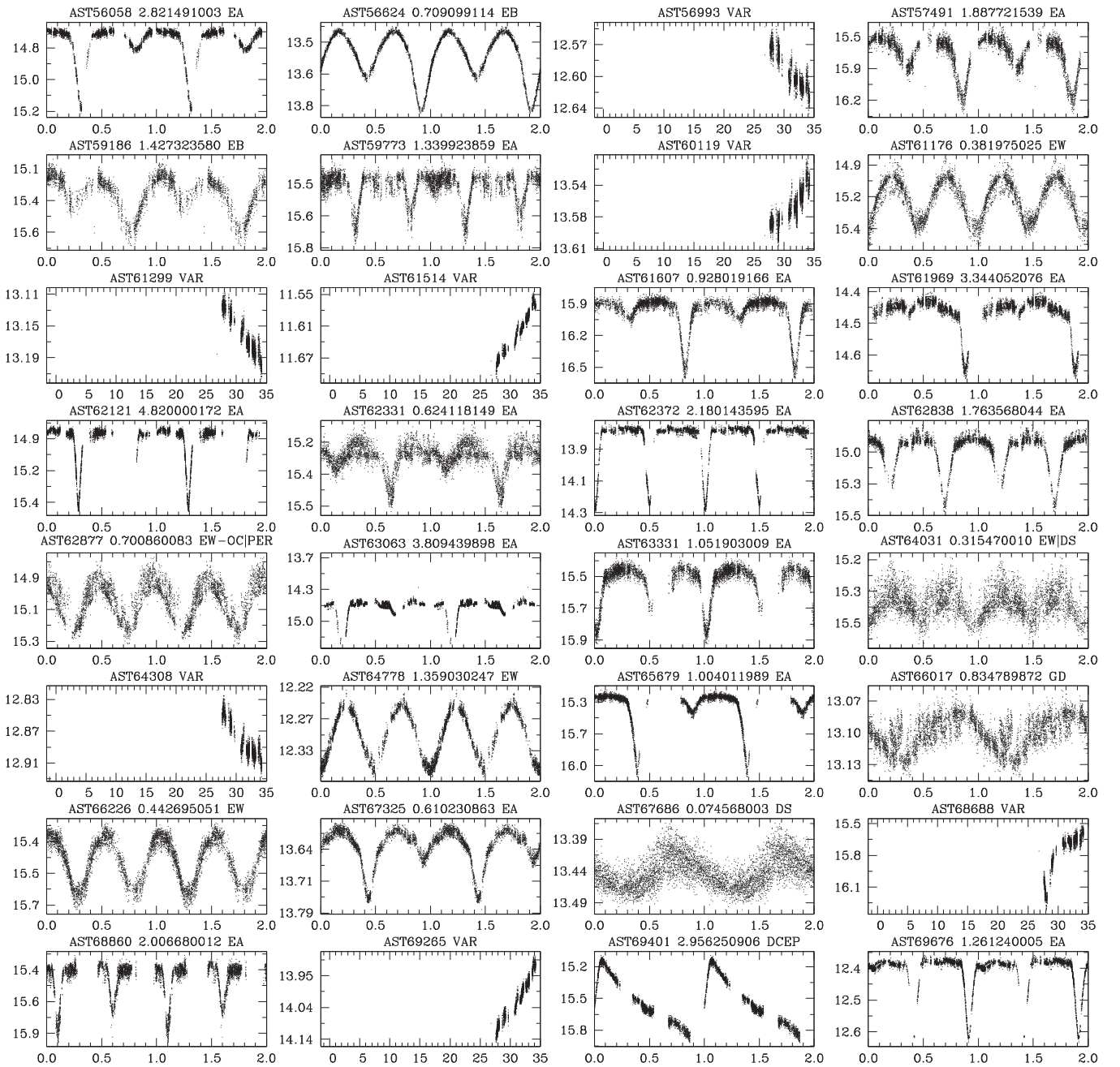


Figure 11. (Continued.)

largest amplitudes in Table 2, are shown in the four panels of Figure 9. AST68688 and 40957 have shown fast rising variability, i.e., ~ 0.6 mag in 3 days (top panels of Figure 9). AST90095 shows a brightness plateau during its ascending stage (bottom left panel of Figure 9); its variability was detected in the GDS catalog, based on sparse data with large gaps (Hackstein et al. 2015). The new variable AST83717 shows a secondary maximum during its descending stage after its i -band maximum brightness (bottom right panel of Figure 9). More observations are needed for further investigations into these four interesting objects.

4. Summary

We have presented the analysis of an i -band images survey from the AST3-1 telescope toward one Galactic disk field

centered at $l = 289^\circ 6347$, $b = -1^\circ 5718$. We detected 560 variable stars in the field from the time-series photometry of 92,583 stars with i magnitude ≤ 16.5 mag during the eight days of observations. Several methods (LS, BLS, DEBiL, and visual inspection) were used to look for the initial periods, and we adopted the methods that gave the smallest scatter in the phase-folded light curves. We used MCMC simulations based on the harmonic function of the primary period for each variable star to estimate the uncertainty of the period and its median value. For the previously known periodic variable stars, the median periods from the MCMC simulations are highly consistent with those given in the AAVSO database, see Figure 3.

We tentatively classified the 560 variables into 285 eclipsing binaries (EWs, EBs, EAs), 27 pulsating variable stars (δ Scuti, γ Doradus, δ Cepheid variable, and RR Lyrae stars), and 248

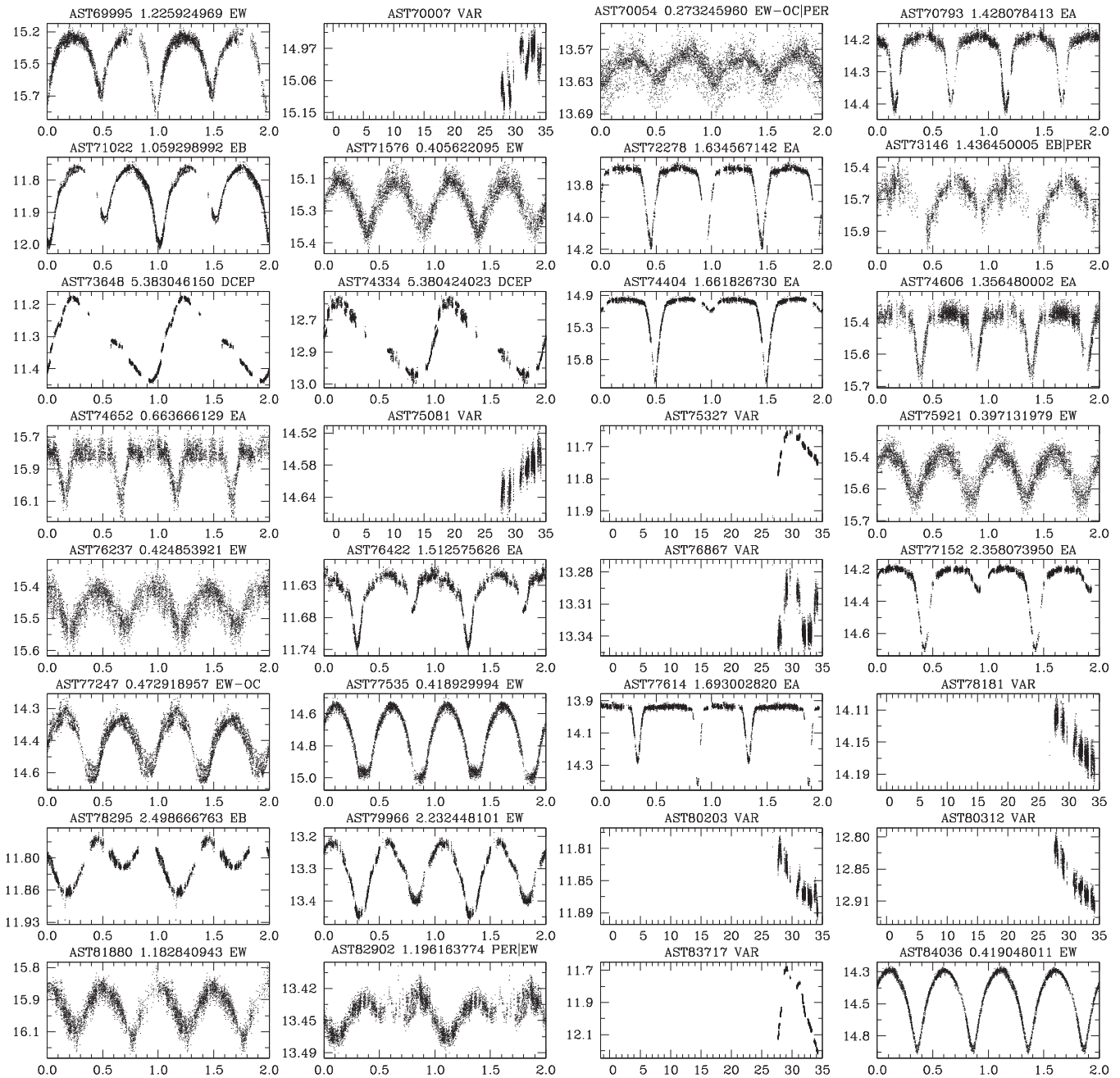


Figure 11. (Continued.)

other types of variables (unclassified periodic, multiperiodic, and aperiodic variable stars). Out of the 560 variables, 339 (61%) are new detections from our data; 42% of the new detections are eclipsing binary stars. We found 34 eclipsing binaries that show O'Connell effects. The interaction between circumstellar matter and the binary components may offer an explanation for the O'Connell effect (see the discussion on AST46538 in Section 3.2.1). We also found one aperiodic variable that shows a plateau light curve and another that shows a secondary maximum after peak brightness. We found one variable in our newly discovered objects with a complex behavior that shows a binary system with an RS CVn-like light-curve morphology; we are in the process of obtaining spectroscopic follow-up observations of this object using the Gemini South telescope. All the time-series data of the variable

stars will be available in the online Journal and via the VizieR Online Data Catalog.²²

We thank Márcio Catelan for helpful discussions and Ricardo Salinas for applying spectral follow-up observations of AST10442. We appreciate comments from the anonymous referees. We thank Lucas Macri for discussions on the Welch-Stetson variability L and Joel Hartman for the discussions on the period uncertainty. This work was supported by the National Basic Research Program (973 Program) of China (Grant Nos. 2013CB834901, 2013CB834900, 2013CB834903), the Chinese Polar Environment Comprehensive Investigation & Assessment Program (Grand No. CHINARE2016-02-03-05), the National

²² <http://vizier.u-strasbg.fr/>

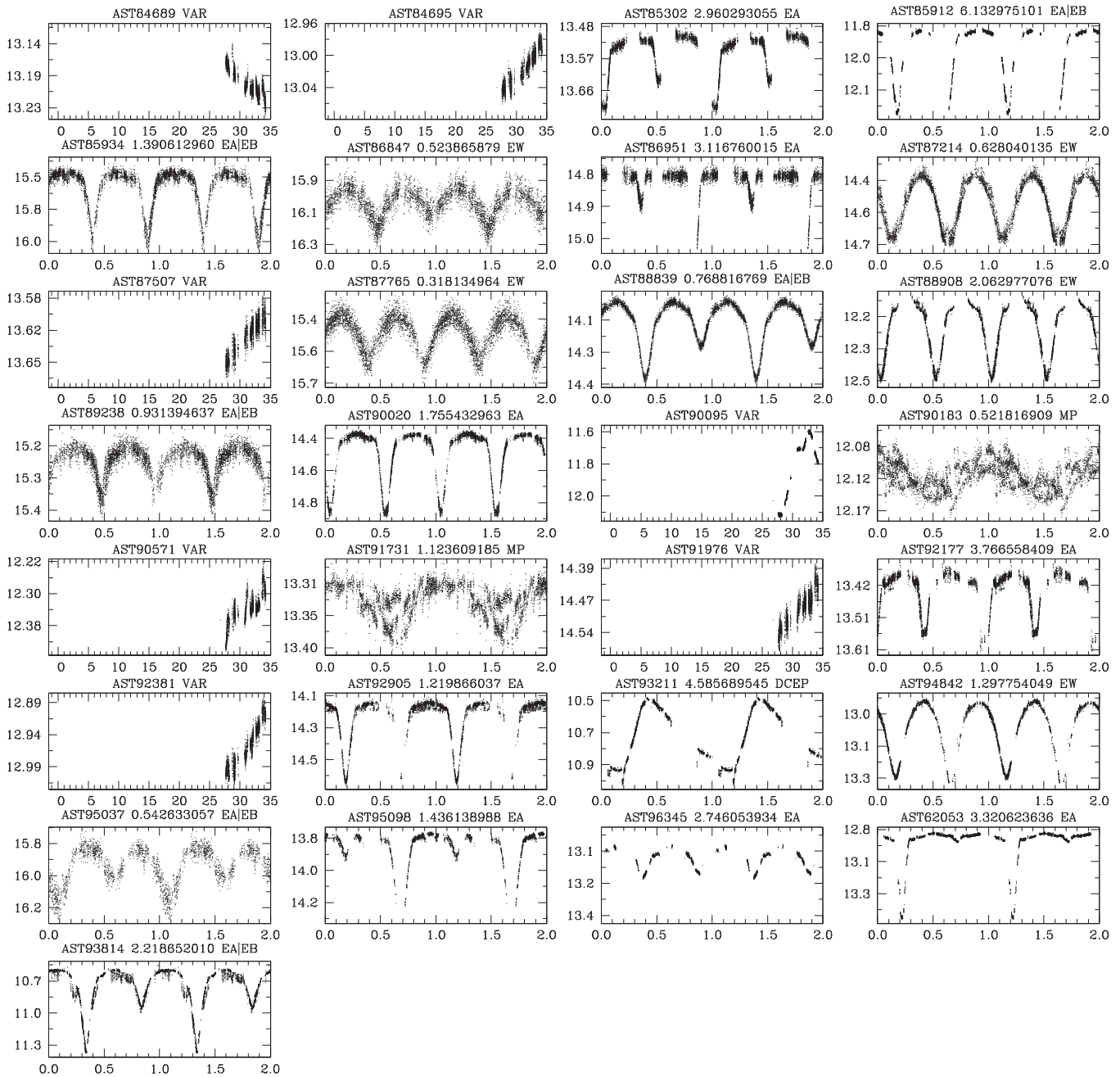


Figure 11. (Continued.)

Natural Science Foundation of China (NSFC grants 11303041, 11203039, 11273019, 11273025, 11403048, 11473038, 11673003), the Australian Antarctic Division, and the National Collaborative Research Infrastructure Strategy (NCRIS). L.Z.W. acknowledges the Chinese Academy of Sciences (CAS), through a grant to the CAS South America Center for Astronomy (CASSACA) in Santiago, Chile and support by the One-Hundred-Talent program of the Chinese Academy of Sciences (034031001). L.F.W. acknowledges the Strategic Priority Research Program “The Emergence of Cosmological Structures” of the Chinese Academy of Sciences, Grant No. XDB09000000. J.N.F. acknowledges the support from the Joint Fund of Astronomy of National Natural Science Foundation of China (NSFC) and Chinese Academy of Sciences through the grant U1231202, the National Basic Research Program of China (973

Program 2014CB845700), and the LAMOST FELLOWSHIP supported by Special Funding for Advanced Users, budgeted and administrated by Center for Astronomical Mega-Science, Chinese Academy of Sciences (CAMS). The authors deeply appreciate the great efforts made by the 24–32th Dome A expedition teams, who provided invaluable assistance to the astronomers that set up and maintained the AST3 and the PLATO-A system.

Appendix

We show phased light curves (or simple time-series when the period is not available) for all new variables and previously known stars in Figures 10 and 11.

References

- Aristidi, E., Fossat, E., Agabi, A., et al. 2009, *A&A*, **499**, 955
- Ashley, M. C. B., Bonner, C. S., Everett, J. R., et al. 2010, *Proc. SPIE*, **7735**, 773540
- Ashley, M. C. B. 2013, in IAU Symp. 288, *Astrophysics from Antarctica*, ed. M. G. Burton, X. Cui, & N. F. H. Tohill (Cambridge: Cambridge Univ. Press), **15**
- Bertin, E. 2006, in ASP Conf. Ser. 351, *Astronomical Data Analysis Software and Systems XV*, ed. C. Gabriel et al. (San Francisco, CA: ASP), **112**
- Bertin, E., & Arnouts, S. 1996, *A&AS*, **117**, 393
- Bonner, C. S., Ashley, M. C. B., Cui, X., et al. 2010, *PASP*, **122**, 1122
- Breger, M. 2000, in ASP Conf. Ser. 210, *Delta Scuti and Related Stars*, ed. M. Breger & M. Montgomery (San Francisco, CA: ASP), **3**
- Brooks, S. P. 1998, *Journal of the Royal Statistical Society. Series D (The Statistician)*, **47**, 69
- Burton, M. G. 2010, *A&ARv*, **18**, 417
- Burton, M. G., Zheng, J., Mould, J., et al. 2016, *PASA*, **33**, e047
- Catelan, M., & Smith, H. A. 2015, *Pulsating Stars* (New York: Wiley)
- Chapellier, E., Mékarnia, D., Abe, L., et al. 2016, *ApJS*, **226**, 21
- Crouzet, N., Guillot, T., Agabi, A., et al. 2010, *A&A*, **511**, A36
- Cui, X., Yuan, X., & Gong, X. 2008, *Proc. SPIE*, **7012**, 70122D
- Cutri, R. M., Skrutskie, M. F., van Dyk, S., et al. 2003, *VizieR On-Line Data Catalog: II/246*, 2MASS All-Sky Catalog of Point Sources, **2246**, 0
- Cuypers, J., Aerts, C., De Cat, P., et al. 2009, *A&A*, **499**, 967
- Devor, J. 2005, *ApJ*, **628**, 411
- Ducati, J. R., Bevilacqua, C. M., Rembold, S. B., & Ribeiro, D. 2001, *ApJ*, **558**, 309
- Fitzgerald, M. P. 1970, *A&A*, **4**, 234
- Fu, J. N., Zong, W. K., Yang, Y., et al. 2014, in IAU Symp. 301, *Precision Asteroseismology*, ed. J. A. Guzik et al. (Cambridge: Cambridge Univ. Press), **409**
- Gaulme, P., McKeever, J., Rawls, M. L., et al. 2013, *ApJ*, **767**, 82
- Giordano, C., Vernin, J., Chadid, M., et al. 2012, *PASP*, **124**, 494
- Girard, T. M., van Altena, W. F., Zacharias, N., et al. 2011, *AJ*, **142**, 15
- Gong, X., Wang, L., Cui, X., et al. 2010, in EAS Publications Ser. 40, *Dome A site testing and future plans*, ed. L. Spinoglio & N. Epchtein (Les Ulis: EDP Sciences), **65**
- Hackstein, M., Fein, C., Haas, M., et al. 2015, *AN*, **336**, 590
- Hartman, J. D., & Bakos, G. Á. 2016, *Astron. Comput.*, **17**, 1
- Hartman, J. D., Gaudi, B. S., Holman, M. J., et al. 2008, *ApJ*, **675**, 1254
- Henden, A. A., Templeton, M., Terrell, D., et al. 2016, *VizieR On-Line Data Catalog: II/336*, AAVSO Photometric All Sky Survey (APASS) DR9, **2336**, 0
- Hu, Y., Shang, Z., Ashley, M. C. B., et al. 2014, *PASP*, **126**, 868
- Huang, Z., Fu, J., Zong, W., et al. 2015, *AJ*, **149**, 25
- Huang, Z. H., Fu, J. N., & Zong, W. K. 2013, in EAS Publications Ser. 64, *Setting a New Standard in the Analysis of Binary Stars*, ed. K. Pavlovski, A. Tkachenko, & G. Torres (Les Ulis: EDP Sciences), **401**
- Jia, P., & Zhang, S. 2012, *Proc. SPIE*, **8447**, 84475J
- Jia, P., & Zhang, S. 2013, *RAA*, **13**, 875
- Kaluzny, J., Stanek, K. Z., Krockenberger, M., et al. 1998, *AJ*, **115**, 1016
- Keller, S. C., Schmidt, B. P., Bessell, M. S., et al. 2007, *PASA*, **24**, 1
- Kolbas, V., Pavlovski, K., Southworth, J., et al. 2015, *MNRAS*, **451**, 4150
- Kovács, G., Zucker, S., & Mazeh, T. 2002, *A&A*, **391**, 369
- Krishna Swamy, K. S. 1996, *Astrophysics: A Modern Perspective* (New Delhi: New Age Internat. Publ.)
- Kulesa, C. A., Walker, C. K., Schein, M., et al. 2008, *Proc. SPIE*, **7012**, 701249
- Lascaux, F., Masciadri, E., & Hagelin, S. 2011, *MNRAS*, **411**, 693
- Law, N. M., Kulkarni, S. R., Dekany, R. G., et al. 2009, *PASP*, **121**, 1395
- Lawrence, J. S., Allen, G. R., Ashley, M. C. B., et al. 2008, *Proc. SPIE*, **7012**, 701227
- Lawrence, J. S., Ashley, M. C. B., Burton, M. G., et al. 2006, *Proc. SPIE*, **6267**, 62671L
- Lawrence, J. S., Ashley, M. C. B., Hengst, S., et al. 2009, *RS&I*, **80**, 064501
- Lawrence, J. S., Ashley, M. C. B., Tokovinin, A., & Travoignon, T. 2004, *Natur*, **431**, 278
- Li, X., Wang, D., Xu, L., et al. 2012a, *Proc. SPIE*, **8444**, 84445M
- Li, Y., Zheng, J., Tuthill, P., et al. 2016, *PASA*, **33**, e008
- Li, Z., Yuan, X., Cui, X., et al. 2012b, *Proc. SPIE*, **8444**, 84441O
- Liang, E.-S., Wang, S., Zhou, J.-L., et al. 2016, *AJ*, **152**, 168
- Liu, Q.-Y., & Yang, Y.-L. 2003, *ChJAA*, **3**, 142
- Lomb, N. R. 1976, *Ap&SS*, **39**, 447
- LSST Science Collaboration, Abell, P. A., Allison, J., et al. 2009, arXiv:0912.0201
- Ma, B., Shang, Z., Hu, Y., et al. 2014, *Proc. SPIE*, **9154**, 1
- Ma, B., Shang, Z., Wang, L., et al. 2012, *Proc. SPIE*, **8446**, 6
- Mékarnia, D., Guillot, T., Rivet, J.-P., et al. 2016, *MNRAS*, **463**, 45
- Meng, Z., Zhou, X., Zhang, H., et al. 2013, *PASP*, **125**, 1015
- Milone, E. E. 1968, *AJ*, **73**, 708
- Moore, A., Allen, G., Aristidi, E., et al. 2008, *Proc. SPIE*, **7012**, 701226
- Nataf, D. M., Stanek, K. Z., & Bakos, G. Á. 2010, *AcA*, **60**, 261
- O'Connell, D. J. K. 1951, *PRCO*, **2**, 85
- Oelkers, R. J., Macri, L. M., Wang, L., et al. 2015, *AJ*, **149**, 50
- Oelkers, R. J., Macri, L. M., Wang, L., et al. 2016, *AJ*, **151**, 166
- Pei, C., Yuan, X. Y., Chen, H. L., et al. 2011, *AcASn*, **52**, 401
- Pei, C., Yuan, X.-Y., Chen, H.-L., et al. 2012, *ChA&A*, **36**, 327
- Pietrukowicz, P., Mróz, P., Soszyński, I., et al. 2013, *AcA*, **63**, 115
- Pojmanski, G. 2005, *yCat*, **50**, 5001
- Qian, S.-B., Wang, J.-J., Zhu, L.-Y., et al. 2014, *ApJS*, **212**, 4
- Rau, A., Kulkarni, S. R., Law, N. M., et al. 2009, *PASP*, **121**, 1334
- Röser, S., Schilbach, E., Schwan, H., et al. 2008, *A&A*, **488**, 401
- Samus, N. N., Durlevich, O. V., et al. 2009, *yCat*, **1**, 2025
- Scargle, J. D. 1982, *ApJ*, **263**, 835
- Schmidt, E. G., Johnston, D., Langan, S., & Lee, K. M. 2004, *AJ*, **128**, 1748
- Shang, Z., Hu, K., Hu, Y., et al. 2012, *Proc. SPIE*, **8448**, 26
- Sims, G., Ashley, M. C. B., Cui, X., et al. 2010, *Proc. SPIE*, **7733**, 77334M
- Sims, G., Ashley, M. C. B., Cui, X., et al. 2012a, *PASP*, **124**, 637
- Sims, G., Ashley, M. C. B., Cui, X., et al. 2012b, *PASP*, **124**, 74
- Smith, H. A. 2004, *RR Lyrae Stars* (Cambridge: Cambridge Univ. Press)
- Soderhjelm, S. 1980, *A&A*, **89**, 100
- Soszyński, I., Poleski, R., Udalski, A., et al. 2008, *AcA*, **58**, 163
- Soszyński, I., Udalski, A., Szymański, M. K., et al. 2008, *AcA*, **58**, 293
- Stetson, P. B. 1996, *PASP*, **108**, 851
- Storey, J. W. V. 2013, in IAU Symp. 288, *Astrophysics from Antarctica*, ed. M. G. Burton, X. Cui, & N. F. H. Tohill (Cambridge: Cambridge Univ. Press), **1**
- Tohill, N. F. H., Kulesa, C. A., Walker, C. K., et al. 2008, in EAS Publications Ser. 33, *Astrophysics from Dome A*, ed. H. Zinnecker, N. Epchtein, & H. Rauer (Les Ulis: EDP Sciences), **301**
- Tremblin, P., Minier, V., Schneider, N., et al. 2011, *A&A*, **535**, A112
- Wang, L., Macri, L. M., Krisciunas, K., et al. 2011, *AJ*, **142**, 155
- Wang, L., Macri, L. M., Wang, L., et al. 2013a, *AJ*, **146**, 139
- Wang, L., Macri, L. M., Wang, L., et al. 2013b, in IAU Symp. 288, *Astrophysics from Antarctica*, ed. M. G. Burton, X. Cui, & N. F. H. Tohill (Cambridge: Cambridge Univ. Press), **320**
- Wang, S., Zhang, H., Zhou, J.-L., et al. 2014a, *ApJS*, **211**, 26
- Wang, S., Zhang, H., Zhou, X., et al. 2015, *ApJS*, **218**, 20
- Wang, S., Zhou, X., Zhang, H., et al. 2012, *PASP*, **124**, 1167
- Wang, S.-H., Zhou, X., Zhang, H., et al. 2014b, *RAA*, **14**, 345
- Watson, C., Henden, A. A., & Price, A. 2016, *VizieR On-Line Data Catalog: B/vsx*, AAVSO International Variable Star Index VSX, **102027W**
- Wei, P., Shang, Z., Ma, B., et al. 2014, *Proc. SPIE*, **9149**, 2
- Welch, D. L., & Stetson, P. B. 1993, *AJ*, **105**, 1813
- Wen, H., Gong, X., & Zhang, R. 2012, *Proc. SPIE*, **8444**, 84445F
- Xu, J., Gong, X., & Gu, B. 2016, *PASP*, **128**, 125004
- Xu, L. 2012, *Proc. SPIE*, **8451**, 845114
- Yang, H., Allen, G., Ashley, M. C. B., et al. 2009, *PASP*, **121**, 174
- Yang, H., Kulesa, C. A., Walker, C. K., et al. 2010, *PASP*, **122**, 490
- Yang, M., Zhang, H., Wang, S., et al. 2015, *ApJS*, **217**, 28
- Yang, Y., Moore, A. M., Krisciunas, K., et al. 2016, arXiv:1610.10094
- Yao, X., Wang, L., Wang, X., et al. 2015, *AJ*, **150**, 107
- Yuan, X., Cui, X., Gu, B., et al. 2014, *Proc. SPIE*, **9145**, 0
- Yuan, X., Cui, X., Liu, G., et al. 2008, *Proc. SPIE*, **7012**, 70124G
- Yuan, X., Cui, X., Su, D.-q., et al. 2013, in IAU Symp. 288, *Astrophysics from Antarctica*, ed. M. G. Burton, X. Cui, & N. F. H. Tohill (Cambridge: Cambridge Univ. Press), **271**
- Yuan, X., Cui, X., Wang, L., et al. 2015, *IAUGA*, **22**, 56923
- Yuan, X., & Su, D.-q. 2012, *MNRAS*, **424**, 23
- Zacharias, N., Finch, C. T., Girard, T. M., et al. 2013, *AJ*, **145**, 44
- Zhou, X., Ashley, M. C. B., Cui, X., et al. 2013, in IAU Symp. 288, *Astrophysics from Antarctica*, ed. M. G. Burton, X. Cui, & N. F. H. Tohill (Cambridge: Cambridge Univ. Press), **231**
- Zhou, X., Fan, Z., Jiang, Z., et al. 2010a, *PASP*, **122**, 347
- Zhou, X., Wu, Z., Jiang, Z., et al. 2010b, *RAA*, **10**, 279
- Zhu, Y., Wang, L., Yuan, X., et al. 2014, *Proc. SPIE*, **9145**, 0
- Zong, W., Fu, J.-N., Niu, J.-S., et al. 2015, *AJ*, **149**, 84
- Zou, H., Zhou, X., Jiang, Z., et al. 2010, *AJ*, **140**, 602